UC Irvine
UC Irvine Electronic Theses and Dissertations

Title
Development of controllable immunostimulants for probing spatiotemporal contributions to immune cell activation mechanisms

Permalink
https://escholarship.org/uc/item/9d96s6n7

Author
Stutts, Lalisa

Publication Date
2015

Peer reviewed|Thesis/dissertation

eScholarship.org Powered by the California Digital Library
University of California

UNIVERSITY OF CALIFORNIA,
IRVINE

Development of controllable immunostimulants for probing spatiotemporal contributions to immune cell activation mechanisms

DISSERTATION

Submitted in partial satisfaction of
the requirements for the degree of

DOCTOR OF PHILOSOPHY

in Chemistry

by

Lalisa Stutts

Dissertation Committee:
Assistant Professor Aaron P. Esser-Kahn, Chair
Professor Kenneth J. Shea
Associate Professor Andrej Luptak

2015

Chapter 1 and 2 © 2015 Wiley-VCH Verlag GmbH & Co.
Chapters 2, 3, and 4 are reproduced in part with permission from *J. Am. Chem. Soc*. **2014**, *136*, 10823. and *ACS Chem. Bio.* **2014**, *9*, 1075. © 2014 American Chemical Society.
All other materials © 2015 Lalisa Stutts

TABLE OF CONTENTS

LIST OF FIGURES

ACKNOWLEDGEMENTS

I thank my committee chair and principle investigator, Professor Aaron Esser-Kahn. Contributing to the development of his new lab at UC Irvine has been an invaluable experience. Thanks, also, to my committee members, Professors Ken Shea and Andrej Luptak, for helpful discussions related to both my qualifying exam and thesis research projects. Additionally, I appreciated the advice and encouragement I received from Professors Greg Weiss and Andy Borovik, and Dr. Carolyn O'Keefe. I acknowledge Professor Zhibin Guan and members of his lab, who gave me my start in graduate research in biomaterials and bioengineering. In particular, Dr. Kanika Chawla, in the brief time working together, was an amazing professional and personal mentor.

From the Esser-Kahn group, I thank my friends and coworkers. Specifically, Nari Ryu and Dr. Rock Mancini were exceptional coauthors, and I greatly appreciated their hard work on our joint projects. Much gratitude goes to Dr. Du Nguyen, Dr. Maya Kleiman, Samantha Goetz, and Kyle Brubaker for their constant support. Thanks, too, to Professor Kasha Slowinska, for bringing both knowledge and laughter to our group. Special thanks to Dr. Troy Moore for being an exceptional lab manager and buddy. I wish them all productive careers and happy lives.

Final thanks go to my family and friends for their positivity and unconditional support. My parents, John and Orapin Stutts, and brother, Marco Stutts, always had an open door and full fridge for me throughout my graduate time. Dr. Nirmal Patel and Dr. Tuwie Nguyen have been awesome friends, despite being many miles away. Señorita Lauren Gaskill has been a supportive friend and roommate. Lastly, thanks to Dr. Dave "Pappy" Shaffer, who has been a great friend and someone I could also always count on for a full fridge (of beer).

Lalisa Stutts

3012 Frederick Reines Hall, Irvine, CA 92697
(714) 299-2070 LStutts@uci.edu

EDUCATION

University of California, *Irvine, CA* Aug. 2010 – Sept. 2015
Ph.D., Chemistry
Research fields: Organic Chemistry and Immunology

Dissertation: "Development of controllable immunostimulants for probing spatiotemporal contributions to immune cell activation mechanisms"

Supported from 2010 to 2011 as a Medicinal Chemistry and Pharmacology Program Fellow (a competitive UCI fellowship). Taught four quarters of undergraduate general chemistry laboratory sections.

Activities and Awards: 2015 Regents' Dissertation Fellow; UCI Chem and Associated Grad Student travel awards recipient; American Chemical Society member; Materials Research Society member; undergraduate student research mentor.

California State University, *Fullerton, CA* Aug. 2005 - Aug. 2010
B.S., Biochemistry
Minor: Political Science

Activities and Awards: 2010 Washington, D.C. Fellow and McCarthy-Potter Fellow, National Academy of Science intern; College of Natural Sciences tutor, peer mentor, and Supplemental Instructor; Student Science Alliance, Organic Chair and Activities Coordinator; Kids-to-College program organizer; 2008 and 2009 summer research stipend recipient.

RESEARCH EXPERIENCE

Graduate Student Researcher, *UC Irvine* July 2011 - Present

Design, synthesis, and characterization of light-responsive immune stimulants toward development of vaccines. Currently investigating the activation mechanisms of single cells and population dynamics of immune cells. Under advisement of Prof. Aaron P. Esser-Kahn.

Graduate Research Rotations, *UC Irvine* Sep. 2010 - June 2011

Rotations through the labs of Profs. Zhibin Guan and Andrej Luptak, synthesizing peptide-saccharide polymers and implementation in 3D culture of stem cells to prolong growth time and drive differentiation; and developing selection techniques for discovering new catalytic RNA, respectively.

Undergraduate Student Researcher, *CSU Fullerton* June 2007 - May 2010

Study of the degradation and toxicity of oxime-containing pharmaceuticals and pesticides in the lab of Prof. Peter de Lijser.

WORK EXPERIENCE

Intern, *National Academy of Sciences, Washington, D.C.* June 2010 - Aug. 2010

Office intern for Government-University-Industry Research Roundtable (GUIRR) within the Policy and Global Affairs Division. Funded through CSU Fullerton and alumni sponsorship. Organized three multi-day meetings (100-200 attendees) to foster communication and relationships between primary researchers, technology developers, funding agencies, and policy makers. Under the mentorship of Susan Sauer Sloan and Dr. Anthony Boccanfuso.

Tutor and Academic Advisor, *CSU Fullerton* Aug. 2006 - May 2010

College of Natural Sciences and Mathematics peer tutor for general and advanced coursework in chemistry, biology, and physics. Advised on academic and personal matters for incoming and transfer students, organized tutoring and group study sessions, worked closely with faculty and staff to develop academic events to promote success in the sciences.

Undergraduate Student Instructor, *CSU Fullerton* Aug. 2009 - May 2010

Teaching assistant and weekly discussion leader for upper division Physical Chemistry course. Generated assignments and exams to reflect curriculum.

SKILLS

Computer: Microsoft Excel/Word/PowerPoint, Adobe Illustrator/Photoshop, ChemDraw, SciFinder, ImageJ

Leadership: exceptional communication, oral speaking, and mentoring skills

Language: English (native)

Advanced chemistry and biology methods

- nuclear magnetic resonance (NMR)
- ultraviolet-visible spectroscopy (UV-Vis)
- high-performance liquid chromatography (HPLC) and liquid chromatography-mass spectrometry (LCMS)
- mammalian cell culture
- biochemical assays
- immunohistochemistry and flow cytometry
- single- and multi-photon confocal microscopy

PUBLICATIONS

Stutts, L., Esser-Kahn, A.P. A light-controlled TLR4 agonist selectable activation of cell subpopulations. *Chem. Bio. Chem.* **2015**, *16*, 1744. **DOI:** 10.1002/cbic.201500164

Mancini, R.J., **Stutts, L.**, Moore, T., Esser-Kahn, A.P. Controlling the origins of inflammation with a photo-active lipopeptide immunopotentiator. *Agnew. Chem. Int. Ed.* **2015**, *54*, 5962. **DOI:** 10.1002/anie.201500416

Ryu, K., **Stutts, L.**, Tom, J.K., Mancini, R.J., Esser-Kahn, A.P. Stimulation of innate immune cells by light-activated TLR7,8 agonists. *J. Am. Chem. Soc*. **2014**, *136*, 10823–10825. **DOI:** 10.1021/ja412314j

Mancini, R.J., **Stutts, L.**, Tom, J.K., Ryu, K., Esser-Kahn, A.P. Directing the immune system with chemical compounds. *ACS Chem. Bio.* **2014**, *9*, 1075-1085. **DOI:** 10.1021/cb500079s

Chawla, K., Yu, T., **Stutts, L.**, Yen, M., Guan, Z. Modulation of chondrocyte behavior through tailoring functional synthetic saccharide-peptide hydrogels. *Biomaterials.* **2012**, *33*, 6052-6060. **DOI:** 10.1016/j.biomaterials.2012.04.058

SELECTED PRESENTATIONS

Stutts, L., Ryu, K. Esser-Kahn, A.P. Tethered and Caged Agonists for Probing Cooperation in Immune Cell Activation. *248th ACS National Meeting*, San Francisco, CA, August 10-14, 2014. (poster presentation)

Stutts, L., Ryu, K. Esser-Kahn, A.P. Development of Photo-Caged Agonists for Probing Synergies in Immune Activation. *Spring Materials Research Society Meeting*, San Francisco, CA, April 21-25, 2014. (oral presentation)

Stutts, L., Esser-Kahn, A.P. Novel Method for Creating Controlled *In Vitro* Prevascularized Hydrogel Networks. *243th ACS National Meeting*, San Diego, CA, March 25-29, 2012. (poster presentation)

DISSERTATION ABSTRACT

Development of controllable immunostimulants for probing spatiotemporal contributions to immune cell activation mechanisms

By

Lalisa Stutts

Doctor of Philosophy in Chemistry

University of California, Irvine, 2015

Professor Aaron P. Esser-Kahn, Chair

Toll-like receptors (TLRs) on innate immune cells are important in the early detection of pathogens and initiation of immune responses. Spatial and temporal aspects of signaling via these receptors are critical in defining unique and effective immune responses. These factors, however, are not well-characterized and there are currently no methods yet to probe them. Herein, I describe approaches developed by the Esser-Kahn lab to address spatial and temporal activation of immune pathways. We have designed photo-labile immunostimulants for controlled activation of cells in space and time. Variants of pyrimido indoles (TLR4 agonist), imidazoquinolines (TLR7 and 8 agonists), and palmitylated-peptides (TLR1, 2, and 6 agonist) were generated with photo-labile protecting groups installed at moieties necessary for productive receptor interaction. We demonstrate controlled activation using light of the NF-κB pathway in RAW macrophages, bone marrow-derived dendritic cells, and TLR-bearing fibroblasts.

CHAPTER 1: Introduction

Overview of the immune system

The focus of this work surrounds innate immune cell mechanisms, specifically, the initial events of molecular recognition of pathogens by Toll-like receptors (TLRs) and subsequent activation of immune pathways. Before discussion of the methods I have developed in the Esser-Kahn group, I first give an overview of the innate immune system.

The innate immune system

The immune system protects us from harmful pathogens by recognizing and responding to foreign bacterial or viral components. The immune system is divided into the innate and adaptive systems. The innate immune system is the first line of defense against an infection. Innate cells, including dendritic cells (DCs), macrophages, natural killer cells, etc., are critical for the early detection of an infection and initial signaling to other immune cells. Recognition of foreign components originating from bacteria, viruses, or fungi is signaled by receptors on or within these innate cells. Binding of pathogenic molecules to the receptors promotes immune pathway activation. Innate cells signal to other innate cells to fight and clear pathogens, and also to adaptive immune cells through cytokine release and antigen presentation. Adaptive cells, including B and T cells, generate a long-term response by synthesizing antibodies that recognize pathogenic antigens. This communication between the two systems is integral for creating appropriate short- and long-term responses to pathogens.

The primary objective of innate immune cells is to recognize foreign, harmful pathogens and propagate the initial response to the other immune cells. In identifying pathogens, immune

cell receptors need to distinguish "self" from "non-self" molecules. Endogenous molecules originate from non-infectious sources, such as damaged or tumorous tissues. These molecules, referred to as damage-associated molecular patterns (DAMPs), are generally nuclear or cytosolic components from the host, including DNA, RNA, purine-based metabolites, and host proteins.[1] Recognition of these self molecules is important in immunity because it alerts the body when there's an injury and initiates the clearing and rebuilding of tissues. Additionally, the innate and adaptive systems use this recognition to provide for continual surveillance and removal of developing tumors.

The immune system's response to exogenous molecules is as, if not more, important than the self recognition aspect. Non-self molecules come from foreign, infectious sources, such as bacteria, viruses, and fungi. Immune cells recognize all types of components from foreign cell surfaces, cytoplasms, and nuclei. These immune cell agonists are known as pathogen-associated molecular patterns (PAMPs), and include small molecules, peptides, proteins, sugars, lipids, and nucleic acids. Recognition of PAMPs is conferred through pattern recognition receptors (PRRs) on or within innate immune cells, which elicit immune pathway activation.

There are four subclasses of PRRs that are involved in the innate immune system: the Toll-like receptors (TLRs), C-type lectin receptors (CLRs), NOD-like receptors (NLRs), and RIG-like receptors (RLRs).[2] Each plays different roles in the immune system and has varying expression levels in different immune cells. TLRs and NLRs are key in the early stages of pathogen recognition and initiation of the innate immune response. CLRs are also crucial for pathogen recognition, but additionally serve to internalize and process antigens for signaling to and activation of the adaptive immune system. RLRs primarily function to detect viral infection. While each of the receptor types have unique roles in pathogen detection and immune cell responses,

they also cooperate with one another for more specific and efficient control over immune activation. This concept of immune synergy will be discussed in more detail later in this section.

Toll-like receptors

The Toll-like receptors are the most widely studied class of PRRs. They are heavily expressed in dendritic cells (DCs), where they survey tissues for pathogens. DCs play a major role in the innate immune system through recognition, but also, as a consequence of activation, alert the adaptive immune system though inflammatory signals and antigen presentation. The outcomes of innate immune activation for the adaptive immune system are highly dependent on which TLRs are activated in an infection.

There are currently ten known TLRs expressed in humans, designated 1,2,…10.[3] These receptors are membrane-bound and located on a cells outer or endosomal membranes. They are horseshoe-shaped receptors that share structural features, including the leucine-rich repeat (LRR) regions and Toll-Interleukin-1-Resistance (TIR) domains. The LRR regions are responsible for the dimerization of receptor monomers upon ligand binding. The TIR domain, located at the receptors cytosolic face, initiates signaling. Upon ligand binding, TLRs dimerize and conformationally shift, to bring the intracellular TIR domains together. These events promote interactions with signaling adapter proteins, MyD88 and TRIF.

TLRs are distinguished by their binding pockets, which interact with different types of agonists.[4] Generally, TLRs that reside on the cell surface recognize structural components from bacteria or fungi (i.e. TLR1, TLR2, and TLR6 bind lipopeptides from Gram-positive bacteria, TLR4 binds lipopolysaccharides from Gram-negative bacteria, etc). Conversely, TLRs that are

found at the endosomal membrane tend to recognize pathogen genetic components (i.e. TLR3 binds dsRNA from bacteria, TLR9 binds ssDNA from bacteria, etc.).

The major pathways involved in innate signaling are the myeloid differentiation primary response gene 88 (MyD88) and TIR-domain containing adapter inducing interferon beta (TRIF) pathways. These pathways are intricate, but are vital for generating unique activation profiles to appropriately respond to each type of pathogen. The result of activation of these pathways is transcriptional level control of inflammatory cytokines and interferons, mainly through the transcription factors nuclear factor kB (NF-κB) and interferon regulating factors (IRFs).

Briefly, all TLRs, except TLR3, signal through the MyD88 pathways (**Figure 1.1**). Upon ligand binding and receptor dimerization, the intracellular TIR domains of the TLRs associate with MyD88 In TLR1/2/6 and TLR4 activation, a second adapter molecule, MyD88-adapter-like (Mal), is also required.[5] Activation of MyD88 recruits Interleukin-1-receptor-associated kinases (IRAK)-4, affording phosphorylation of IRAK-1, and subsequent association with tumor necrosis factor receptor-associated factor (TRAF)-6. TRAF6 activation leads to complexation of TAB2, TAB3, and TAK1. The next step in the signaling cascade is the activation of mitogen-activated protein kinase kinases (MKKs) and Inhibitor of NF-κB kinases (IKKs). Finally, these events lead to the activation of the transcription factors NF-κB, activator protein-1 (AP-1), and cyclic-AMP-responsive element-binding protein (CREB). Activation of transcription factors means they translocate from the cytoplasm to inside the nucleus to exert transcriptional control. These factors, specifically, cause the production of pro-inflammatory cytokines, such as interleukin (IL)-1, IL-12, and tumor necrosis factor α (TNF). Additionally, TLR7, 8, and 9 signal through MyD88 to

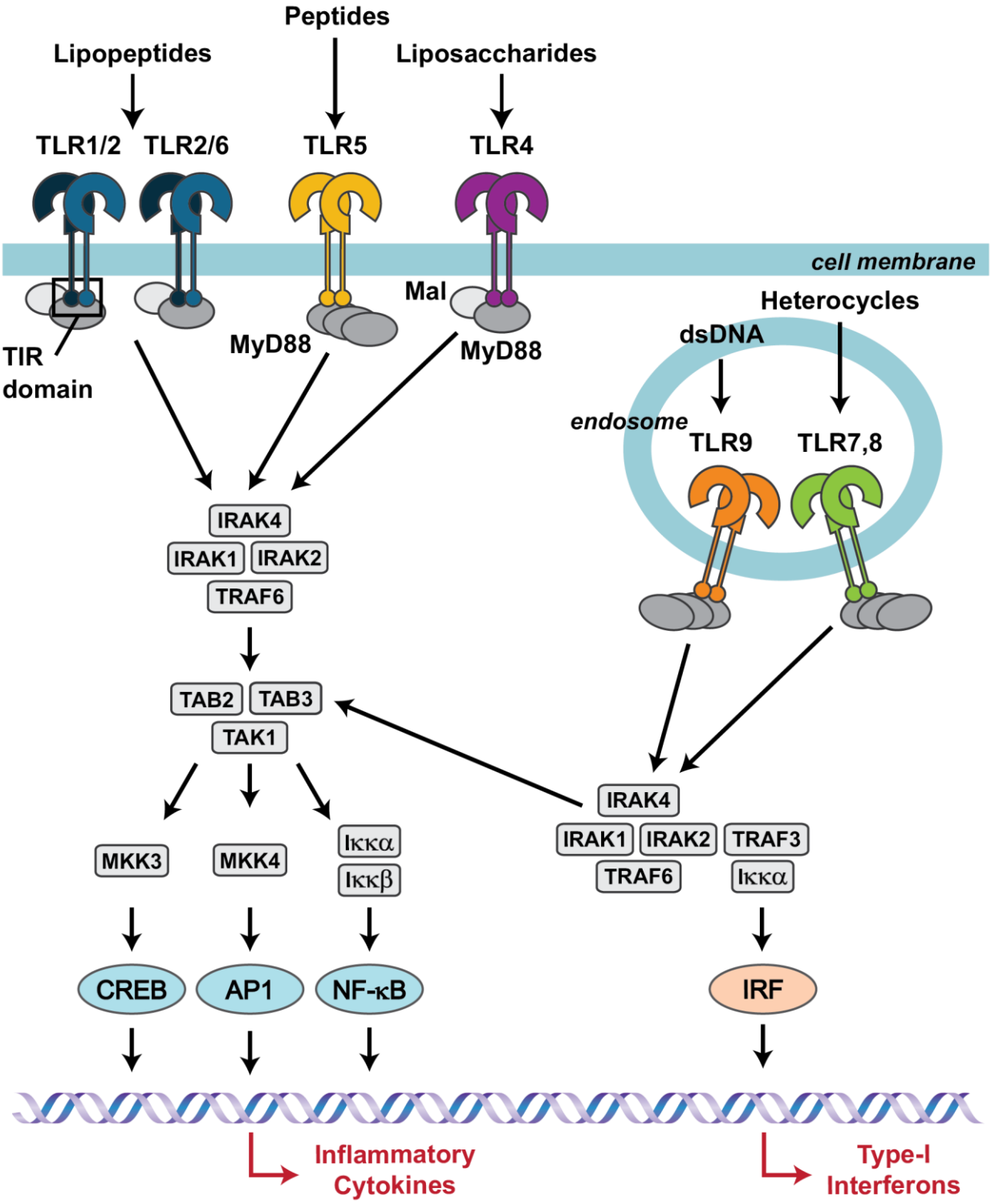

Figure 1.1. MyD88 signaling pathways.

cause IRAK-TRAF-IKK complexation and subsequent activation of the transcription factor IRF7. This factor promotes transcription of interferons (IFN-α and IFN-β).

The second signaling pathway, TRIF, is activated by TLR3 and 4 (**Figure 1.2**). Again, TLR4 requires an adapter, toll-like receptor adapter molecule (TRAM), for signaling.[6] TLR-TRIF association promotes activation of TRAF-3, which interacts with Tank-binding kinase (TBK)-1 and IKK. These kinases then activate the transcription factor IRF3, which induces IFN-β production. Finally, the activation of NF-κB, AP-1, and CREB can also be activated via TRAF3 through receptor-interacting protein (RIP)-1.

Challenges in immunology

Immune activation mechanisms and synergies

Both the innate and adaptive immune systems are critical for protection and survival. Innate immune cells are the first line of defense in these pathways, surveying the body for damage or pathogens, and upon recognition of harmful signals, will begin to eliminate and/or alert other immune cells of the threat. Over the past three decades, much effort has been put into uncovering the biochemical pathways that initiate and propagate signaling in immune cells in response to pathogens. As discussed, the major mode of pathogen recognition is through Toll-like receptors, which signal through the MyD88 and/or TRIF pathways to ultimately produce inflammatory cytokines and interferons. The next challenge in immunology is to elucidate how these pathways operate together intra- and intercellularly to then effect diverse responses and efficient activation of the immune system.

The prevailing theory on how a small number of PRRs is able to detect and afford such diversity in response types and intensities is synergy. Immune synergies, sometimes called

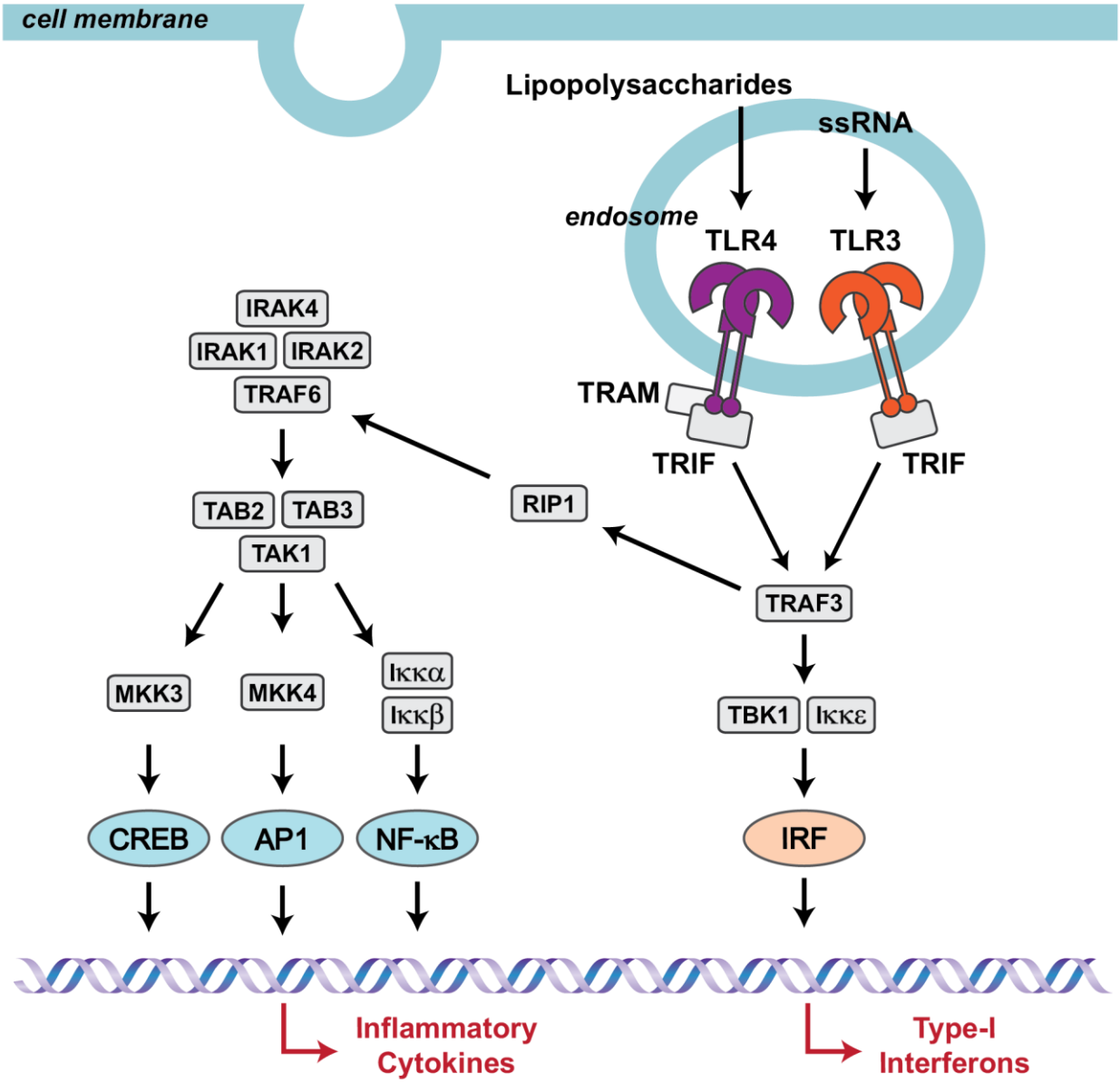

Figure 1.2. TRIF signaling pathways.

inflammatory networks, generally refer to the cooperation that occurs between cells, pathways, or agonists that afford a greater than additive response. Unlike initial models of immune stimulation, where a single pathogenic ligand would bind and activate one type of receptor to initiate a response, this more encompassing and dynamic model of activation synergy takes into account that numerous types of pathogenic ligands bind multiple receptors to initiate a complex network of immune pathways. This is believed to result in a potent and unique response.[7] Immune synergies have been observed in many instances, including via high-throughput screening and vaccine models, whereby cells are treated with multiple immunostimulants to enhance immune activity and immunogenicity of an antigen.[8,9]

Spatial and temporal factors in immune activation

The biochemical pathways that make up an organism are extensive and complex. Though often portrayed as linear pathways, they are extremely dynamic and, as such, highly dependent and spatial and temporal aspects of signaling. The immune-related pathways, as outlined above, are just as complicated and ill-defined. The first steps in understanding these spatial and temporal contributions was to discover which pathways are primarily responsible for activation and what stimulates them. Recent work in adjuvant design has determined that immune cells co-treated with multiple agonists results in distinct and heightened immune profiles.[9,10] The current methods for activating the immune system are basically to treat an animal or cell *in vitro* in bulk with one or more immunostimulants. Approaches that control agonists exposure and activation in space and time are limited. Generally, agonists are added to cells manually and sequentially, or by application to different areas of an animal (i.e. dermal versus injection). There are some recent examples of agonist- and/or antigen-loaded nanomaterials for slow release treatments.[11–13] These constructs do enhance immune activation, however, have some drawbacks in probing spatial and temporal

mechanisms, including time-consuming or complicated synthesis and, most importantly, limited controllability *in vitro* and *in vivo.*

A method for uncovering the sources of immune synergies

The Esser-Kahn group has developed a method for studying immune synergies. We took inspiration from the field of neurobiology, which has probed spatial and temporal elements of signaling for over three decades through the use of light-activated molecules.[14–19] In this work, I describe the development of three novel immunostimulants and their applications in probing spatial and temporal factors in immune cell activation. These agonists are all based on small molecule TLR immunostimulants: pyrimido indole (TLR4 agonist), imidazoquinoline (TLR7 and 8 agonist), and palmitylated-cysteine-serine-tetralysine (TLR2 and 6 agonist). We generated controllable variants of these agonists by installation of photo-labile protecting groups at positions critical for receptor interaction and, therefore, activity. These caged compounds are unable to productively interact with the receptor until deprotection with UV light.

The aims of this work were to 1. design and synthesize light-controlled immunostimulants, 2. demonstrate their utility in applications of spatially- and temporally-controlled immune activation, and 3. make progress towards understanding complex immune signaling and synergies.

References

(1) Rubartelli, A.; Lotze, M. T. *Trends Immunol.* **2007**, *28* (10), 429–436.
(2) Akira, S.; Uematsu, S.; Takeuchi, O. *Cell* **2006**, *124* (4), 783–801.
(3) Akira, S.; Takeda, K. *Nat. Rev. Immunol.* **2004**, *4* (7), 499–511.
(4) Mancini, R. J.; Stutts, L.; Ryu, K. A.; Tom, J. K.; Esser-Kahn, A. P. *ACS Chem. Biol.* **2014**, *9* (5), 1075–1085.
(5) O'Neill, L. A. J.; Dunne, A.; Edjeback, M.; Gray, P.; Jefferies, C.; Wietek, C. *J. Endotoxin Res.* **2003**, *9* (1), 55–59.
(6) Kagan, J. C.; Su, T.; Horng, T.; Chow, A.; Akira, S.; Medzhitov, R. *Nat. Immunol.* **2008**, *9* (4), 361–368.
(7) Parker, L. C.; Prince, L. R.; Sabroe, I. *Clin. Exp. Immunol.* **2007**, *147* (2), 199–207.
(8) Garcia-Cordero, J. L.; Nembrini, C.; Stano, A.; Hubbell, J. A.; Maerkl, S. J. *Integr. Biol.* **2013**, *5* (4), 650.
(9) Guy, B. *Nat. Rev. Microbiol.* **2007**, *5* (7), 505–517.
(10) Napolitani, G.; Rinaldi, A.; Bertoni, F.; Sallusto, F.; Lanzavecchia, A. *Nat. Immunol.* **2005**, *6* (8), 769–776.
(11) Maldonado, R. A.; LaMothe, R. A.; Ferrari, J. D.; Zhang, A.-H.; Rossi, R. J.; Kolte, P. N.; Griset, A. P.; O'Neil, C.; Altreuter, D. H.; Browning, E.; Johnston, L.; Farokhzad, O. C.; Langer, R.; Scott, D. W.; von Andrian, U. H.; Kishimoto, T. K. *Proc. Natl. Acad. Sci.* **2015**, *112* (2), E156–E165.
(12) Gu, L.; Ruff, L. E.; Qin, Z.; Corr, M.; Hedrick, S. M.; Sailor, M. J. *Adv. Mater.* **2012**, *24* (29), 3981–3987.
(13) Kwong, B.; Liu, H.; Irvine, D. J. *Biomaterials* **2011**, *32* (22), 5134–5147.
(14) Banghart, M.; Borges, K.; Isacoff, E.; Trauner, D.; Kramer, R. H. *Nat. Neurosci.* **2004**, *7* (12), 1381–1386.
(15) Aravanis, A. M.; Wang, L.-P.; Zhang, F.; Meltzer, L. A.; Mogri, M. Z.; Schneider, M. B.; Deisseroth, K. *J. Neural Eng.* **2007**, *4* (3), S143–S156.
(16) Adamantidis, A. R.; Zhang, F.; Aravanis, A. M.; Deisseroth, K.; de Lecea, L. *Nature* **2007**, *450* (7168), 420–424.
(17) Wyart, C.; Bene, F. D.; Warp, E.; Scott, E. K.; Trauner, D.; Baier, H.; Isacoff, E. Y. *Nature* **2009**, *461* (7262), 407–410.
(18) Sauers, D. J.; Temburni, M. K.; Biggins, J. B.; Ceo, L. M.; Galileo, D. S.; Koh, J. T. *ACS Chem. Biol.* **2010**, *5* (3), 313–320.
(19) Nguyen, D. P.; Mahesh, M.; Elsässer, S. J.; Hancock, S. M.; Uttamapinant, C.; Chin, J. W. *J. Am. Chem. Soc.* **2014**, *136* (6), 2240–2243.

CHAPTER 2: Light-controlled agonist for TLR4 and spatial and temporal control in TLR signaling

Overview of TLR4 signaling

Receptor structure and agonists

Toll-like Receptor 4 is a critical receptor in innate immune signaling and is the most highly studied receptor of the TLR family. TLR4 is activated by a diverse array of structures, including lipids, peptides and proteins, and small molecules. TLR4 was first discovered as the target receptor of lipopolysaccharide (LPS), a component of the outer membrane of Gram-negative bacteria. Like other TLRs, TLR4 is a membrane-bound, horseshoe-shaped receptor that has leucine-rich repeat (LRR) regions and Toll-Interleukin-1-Resistance (TIR) domains. TLR4 is structurally distinct from other TLRs in that it requires a co-protein, MD2, for functional recognition of agonists and activation. The crystal structure of TLR4 with MD2 and LPS shows that the agonist binding pocket forms between the receptor and co-protein, with the hydrophobic tails of Lipid A inserted into the hydrophobic core of MD2 (**Figure 2.1**).[1] Two such dimers then complex with each other to form a tetramer consisting of two TLR4 and two MD2 subunits. The electrostatic interaction of the 4-phosphate with arginine and lysine residues of TLR4 appears critical for the activity of monophosphoryl Lipid A (MPLA) and all other LPS derivatives.[2]

The native agonist of TLR4, LPS, is composed of Lipid A (a phosphorylated disaccharide with multiple lipid chains) and a long polysaccharide. It has been determined that the phosphorylated Lipid A moiety of LPS is responsible for TLR4 activation. Several derivatives of monophosphoryl Lipid A (MPLA) have been extracted from various bacteria and synthesized, including Eritoran (E5564, an antagonist) and other aminoalkyl glucoaminide 4-phosphates (**Figure 2.2**).[3,4] Reduced forms of MPLA have recently been synthesized, including

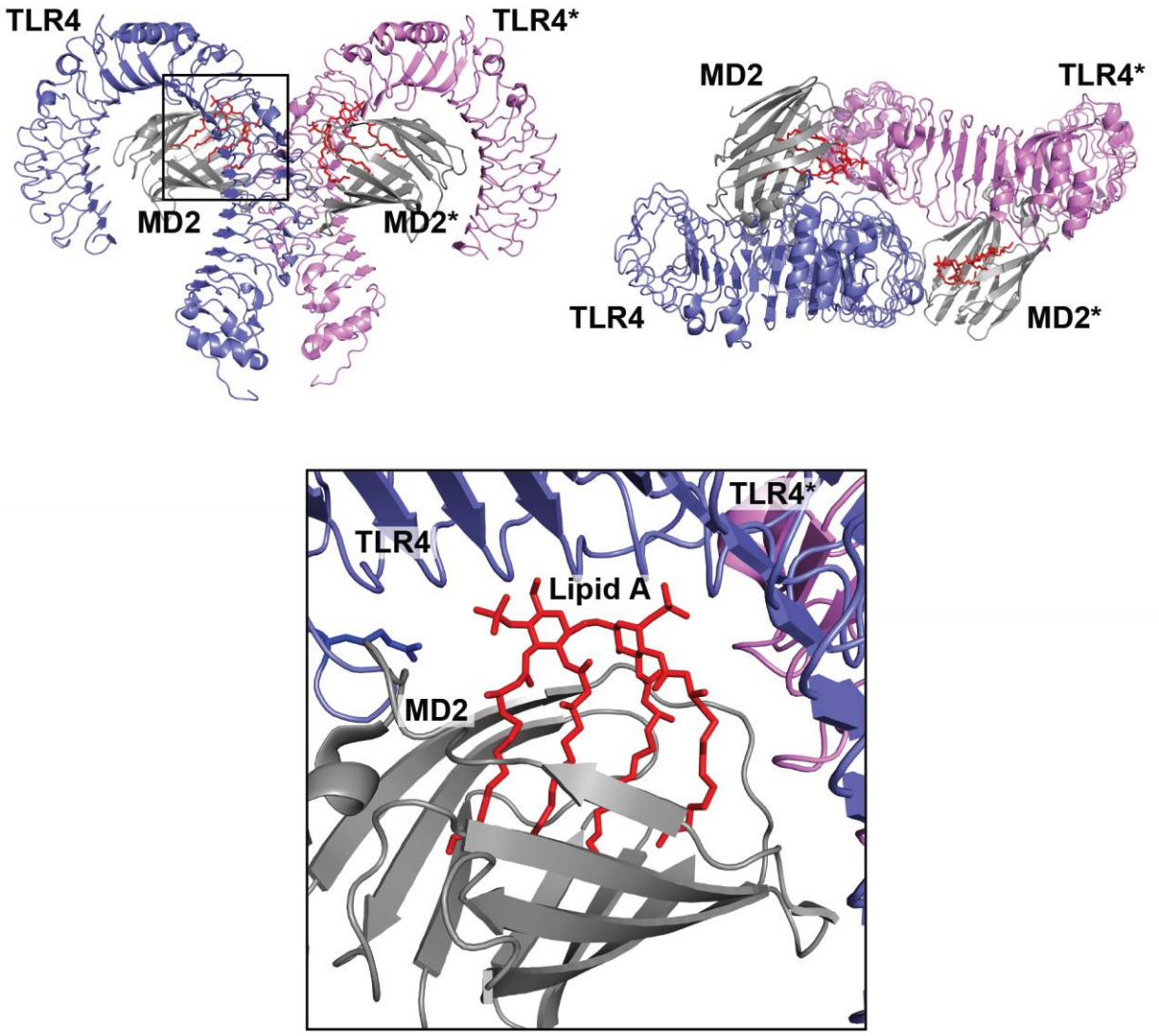

Figure 2.1. Crystal structure of TLR4 with MD2 and lipopolysaccharide (polysaccharide not shown for clarity). LPS binding promotes formation of a heterotetramer of two TLR4 receptors and two MD2 adapter proteins. The lipid chains of lipidated agonists intercalate into MD2, leaving the saccharide head unit to interact with the TLR.

glucopyranosyl Lipid A (GLA).[5] Substitution at the primary alcohol in Lipid A does not seem to interrupt binding, as this is the position connected to the bulky saccharide chain of LPS. Synthetic variants of Lipid A have been an invaluable tool in studying ligand-receptor interactions and immune pathways, as these molecules are characterized and highly pure. Much confusion and debate stemmed from experiments using LPS as an agonist, as bacteria-extracted batches are inherently diverse in their polysaccharide and lipid structures.[6]

While LPS and its derivatives are widely applied in immunological studies, other types of TLR4 agonists have been discovered in recent years. Peptide- and protein-based agonists, with no lipid tail or phosphate moieties can signal through TLR4. One notable example is the activation of TLR4 by Der p 2, a dust-mite protein that causes dust allergies. The mode of action of Der p 2 has not been shown, however, its structural homology to MD2 has been suggested to aid in TLR4 binding.[7,8] Several peptide agonists of TLR4 have been identified via phage display and antibody binding assays, however, it has yet to be determined how these peptides activate TLR4 and whether a co-protein is necessary for binding.[9] Endogenous molecules, such as heat shock proteins 60[10] and 70[11], fibrinogen[12], fibronectin domain A[13], extracellular DNA-binding proteins[14], and other molecules activate TLR4, but the modes of binding are also unclear. With the promiscuity of this TLR, many questions remain in both the design of selective TLR4 ligands, and the mode of action of known agonists.

In addition to lipid and peptide agonists, small molecule TLR4 activators have been uncovered by Cottam and coworkers. Using high-throughput cell-based screening, they identified pyrimido[5,4 *b*]-indoles[15] and 4-aminoquinazolines[16] as highly selective TLR4 agonists (**Figure 2.2**). Through in depth SAR studies, they found that substitutions of the pyrimidoindole and quinazoline cores were as limiting as those derived from Lipid A. Using *in silico* docking studies,

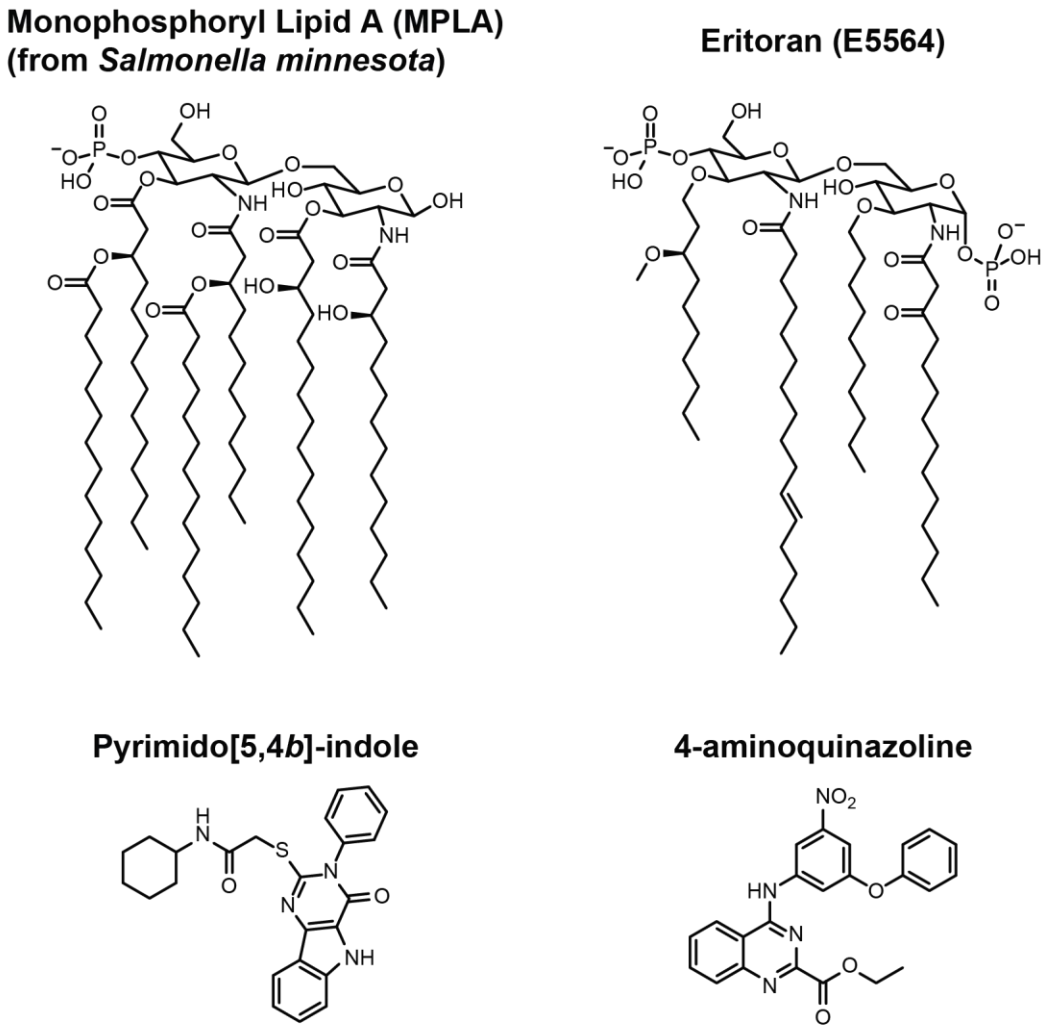

Figure 2.2. Common TLR4 agonists. Truncated variants of LPS include MPLA and eritoran (an antagonist), and are commonly applied in immunological studies. The recently discovered pyrimido indoles and aminoquinazolines represent a new class of small molecule agonists that activate TLR4 via unique binding modes.

they predicted that the indole compounds bind to a unique binding site on the receptor, yet still bring together TLR4 and MD2 and signals through the NF-κB pathway.

TLR4 signaling

The most unique aspect of TLR4 is that it can signal through both the MyD88 and TRIF pathways (**Figure 2.3**). The selectivity in signaling between the two pathways is currently under investigation, though it is known that MyD88 activation occurs at the cell membrane, and switches to the TRIF pathway upon endocytosis of the receptor. Most exciting is that different TLR4 agonists change the signaling pathway from predominately MyD88 to TRIF, implying a structural basis for the activation of these signaling pathways.[17,18] Intriguingly, even the stereo-chemical configuration of the Lipid A moiety of lipopolysaccharide can direct the TLR4 downstream pathway.[19]

The activation outcome of the cell when activated by TLR4 depends on the pathway activated (MyD88 or TRIF). MyD88 activation results in NF-κB, AP1, and CREB transcription factors to be activated, causing the synthesis and release of pro-inflammatory cytokines. TRIF activation results in production of Type I interferons through IRF3. The resulting immune response and its magnitude are proposed to be determined by the balance of the two pathways over time.[20,21] Additionally, we hypothesize that TLR4's dual pathways play a role in immune synergies.

Probing TLR4 activation mechanisms

Despite the strong spatial and temporal components of TLR signaling[22,23], there are few examples of controlling immune cells in time or space[24–26], and no methods yet exist to modulate TLR4 activity. The aim of this work was to generate a controllable agonist that allows us to study

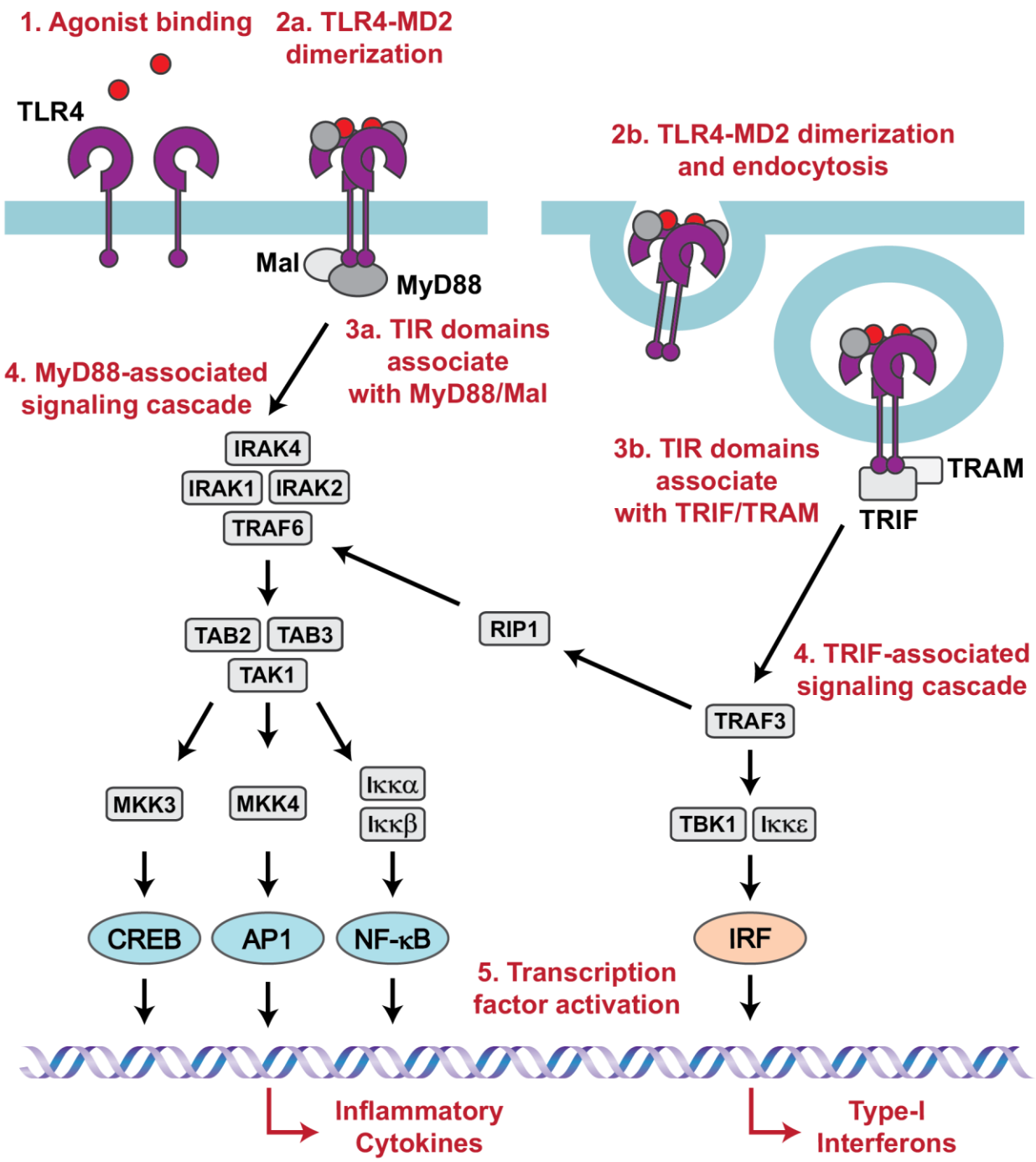

Figure 2.3. TLR4 signaling pathways. Activation of TLR4 results in signaling of both MyD88 and TRIF pathways, whereby pathway switching is dependent of the immunostimulant and endocytosis of the receptor complex. These pathways leads to activation of both inflammatory cytokines and interferons.

the spatial and temporal contributions of TLR activation. Control over the agonist was achieved by protection with a photo-labile protecting group at a position on the agonist critical for receptor interaction and, therefore, activity (**Figure 2.4**). The compound, when protected, would be unable to interact with the receptor; however, upon deprotection with light, the agonist can appropriately bind TLR4 to initiate the signaling cascade. The goal of this work was to create the first controllable TLR4 agonist and simply demonstrate its utility in spatial activation. Here, we investigated the spatial aspects of immune activation by selectively stimulating populations of cells.

The agonist chosen for this method was the TLR4 immunostimulant, pyrimido[5,4 *b*]-indole. Unlike the native lipopolysaccharide and related agonists, this small molecule can be easily synthesized in gram quantities and is easier to handle and characterize. In addition, the structure-activity relationship (SAR) study of these molecules were thoroughly studied.[15] The indole nitrogen did not tolerate substitution and, as a functional handle, could be easily modified with a protecting group. Furthermore, *in silico* docking studies predict a hydrogen bonding interaction between the indole NH and glutamic acid residue-349 of TLR4.[15] Modification of the indole at that position would, therefore, interrupt the receptor binding of the agonist. Thusly, we chose the indole nitrogen as the site to install the photo-labile cage, 6-nitroveratryloxycarbonyl (NVOC). Upon exposure to longwave UV light (NVOC λ_{max} = 340 nm), this protecting group is cleaved to form the active TLR4 agonist. Activation was assessed by NF-κB assays in TLR4-bearing cells.

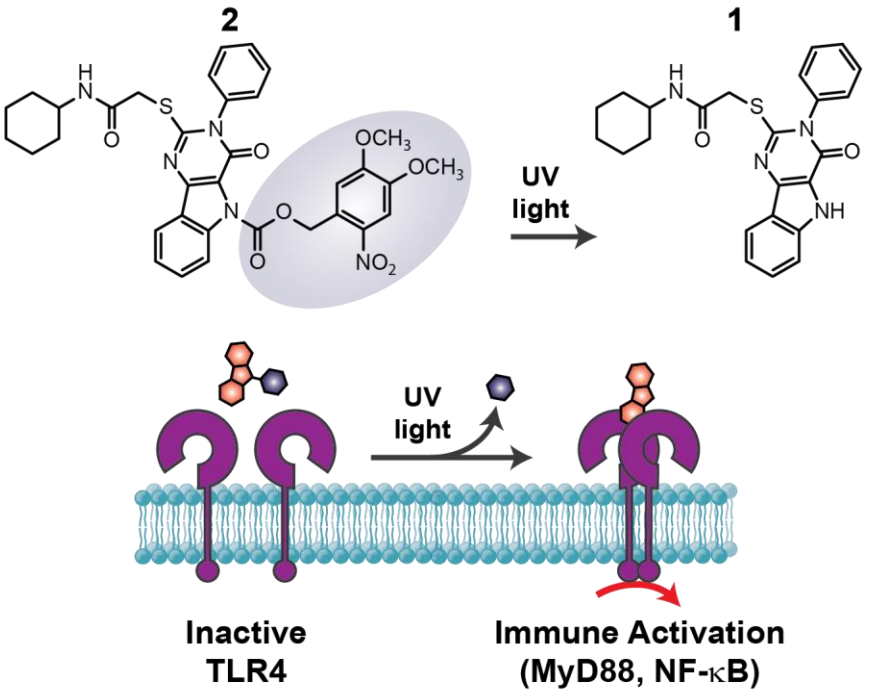

Figure 2.4. Photo-controlled deprotection of caged TLR4 agonist. NVOC-caged pyrimido[5,4-*b*]indole **2** is converted to **1** using UV light (365 nm) to activate immune cells via TLR4.

Design and characterization of a caged TLR4 agonist

Synthesis of the TLR4 agonist and caged agonist

Our development of a light-controlled TLR4 agonist began with the synthesis of the active small molecule TLR4 agonist, pyrimido[5,4-*b*]indole **1**, as described previously.[15] The caged TLR4 agonist was generated by NVOC-protection of **2** (**Appendix A**). Briefly, **2** was generated by deprotonating the indole amine of **1** (200 mg, 0.46 mmol) with NaH (60% dispersed in mineral oil, 100 mg, 2.5 mmol) in THF (2 mL), followed by addition of 6-nitroveratryl chloroformate (251 mg, 0.91 mmol) in THF (10 mL). The mixture was heated to reflux for 3 h. The reaction was quenched with water and the product was extracted with excess methylene chloride and purified by silica gel column chromatography to obtain **2** in 65.5% yield. Protection at the indole nitrogen was confirmed *via* high-resolution mass spectrometry, and ^{1}H and ^{13}C NMR spectroscopy (**Appendix B**).

Characterization of deprotection

The deprotection efficiency of **2** was established by UV absorption, combined with HPLC analysis of **1** and **2** before and after light exposure. A long wave UV hand lamp (15 W, 365 nm) was used as the light source. The UV absorption spectrum of **1** ranges from 250 to 360 nm with two local maxima at 250 and 280 nm (**Figure 2.5**). The spectrum of **2** exhibits only the peak at 250 nm. Following exposure of **2** to UV light for 30 min, a peak in the spectrum appears at 280 nm though it did not increase in intensity with further exposure.

The presence of **1** following light exposure of **2** was confirmed by HPLC analysis (**Figure 2.6**). In these data, **1** and **2** were pure and had elution times of 13.5 and 17.1 min, respectively. Confirmation of these LC peaks were performed using mass spectrometry. The compound with an

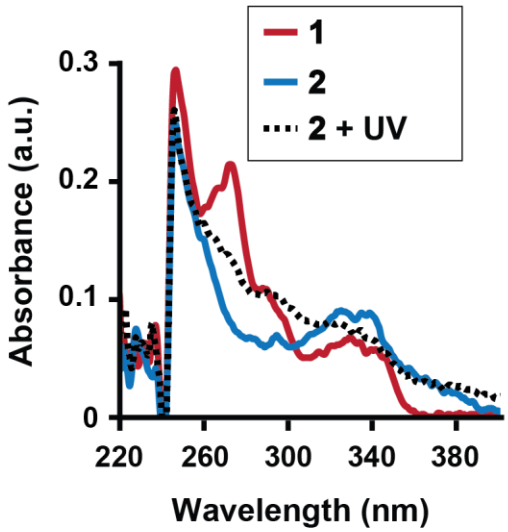

Figure 2.5. Deprotection of the cage on **2** with UV light affords the agonist **1**. Deprotection was observed by UV-Vis absorption of **2** before (solid blue line) and after 30 min light exposure (15 W, 365 nm, dashed black line), as compared to **1** (solid red line).

elusion time of 13.5 min corresponded to ($M_{TLR4\ agonist}$+1) = 433, and the compound with an elusion time of 17.1 min corresponded to ($M_{caged\ agonist}$+1) = 640. The amount of each species was quantified by integrating the area under the correlated LC peak. For solutions where **2** was not exposed to UV light, **1** was not detected. For solutions of **2** exposed to UV light, the peak at 17.1 min decreased, and the peak at 13.5 min appears and grows with increased exposure to UV light up to 30 min. Conversion of **2** to **1** reached a maximum of 57% after 30 min of UV light exposure (**Figure 2.7**). HPLC and mass spectrometry analysis of **2** after exposure to UV light showed that **1** was the major species and that minimal byproducts had formed. The limited conversion is due to a fraction of caged compound that does not readily deprotect under the mild conditions used.

Activation of cells using light

Preliminary assessment of immune activation

We confirmed that photo-deprotection of the caged agonist translated to light-controlled activation of TLR4 by testing **2** on a model cell line bearing TLRs—RAW-Blue macrophages. These cells express the TLR4 signaling machinery and a secreted embryonic alkaline phosphatase (SEAP) reporter for NF-κB activation (**Figure 2.8**). SEAP levels are monitored using a detection medium, QUANTI-Blue, affording a colorimetric readout of TLR activation. This assay served as an initial examination of immune activity of the unmodified **1** and caged **2** agonists, and was not employed to examine spatial or temporal activation. Based on the previous SAR study of **1**[15] and our deprotection characterization of **2**, we predicted that **1** and **2** after UV light exposure, would affect immune activity, while **2** without UV light exposure, would have little to no effect on NF-κB activity in cells.

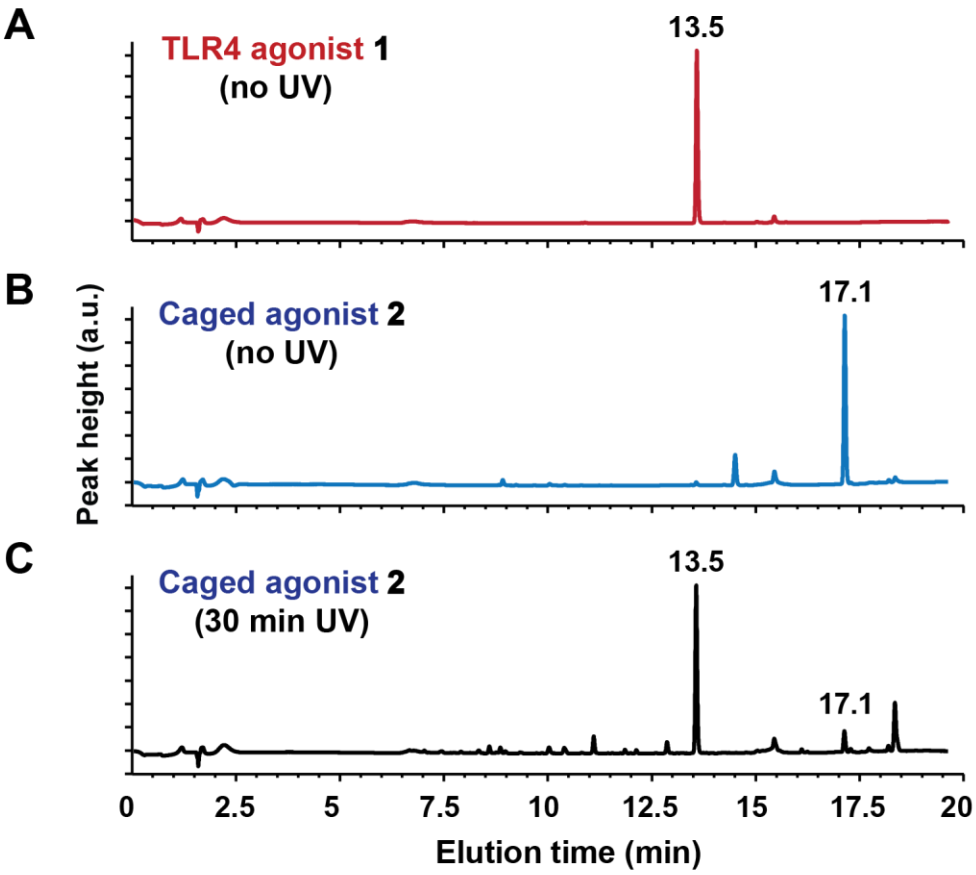

Figure 2.6. Deprotection of the cage on **2** with UV light affords the agonist **1**. HPLC traces of **1** (**A**, red line) and **2** before (**B**, blue line) and after 30 min UV exposure (**C**, 15 W, 365 nm, black line). Samples were eluted using an acetonitrile and water gradient varying from 10:90 to 90:10 (ACN:H_2O) over 20 min at a rate of 5 mL/min. The detector was set at 250 nm for the signal acquisition. **1** had an elusion time of 13.5 min (**A**), and **2** had an elusion time of 17.1 min (**B**).

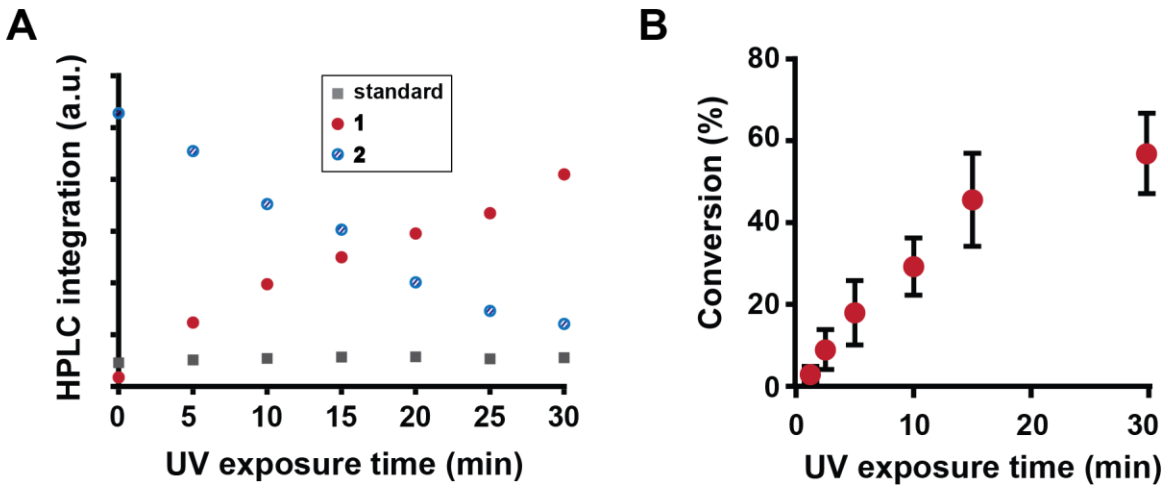

Figure 2.7. Deprotection of the cage on **2** with UV light affords the agonist **1**. HPLC integrations of the major components in a solution of **2** after 30 min UV exposure (15 W, 365 nm (**A**). Aliquots were taken every 5 min of light exposure and combined with an internal standard, methyl indole-5-carboxylate, then chararcterized by HPLC analysis. Integrations corresponding to the eluted compounds are plotted: **1** (red circle), **2** (blue striped circle), and the internal standard (gray square).Percent conversion (**B**) of **2** to **1** following light exposure (15 W, 365 nm) was determined by HPLC analysis. Conversion of the caged agonist reaches 57% after 30 min of UV light exposure.

RAW-Blue cells were treated with **1** and **2** (10 μM), then exposed to UV light (15 W, 365 nm) for 10 min. The cells were incubated for 18 h before the culture supernatant was analyzed to determine NF-κB activation. We observed the selective activation of cells upon UV light exposure (**Figure 2.9**). Treatment with **2** and exposure to UV light yielded NF-κB activity equivalent in concentration to the TLR4 agonist **1**. This result was most clearly seen using 10 μM agonist, and is consistent with previous concentration screens of **1**, which show a non-linear relationship of concentration and NF-κB activity.[15] A challenge in innate immunity is that agonist concentration is not an absolute measure of immune cell activity. As such, the deprotection kinetics measured cannot be directly related to cell experiments and immune activity. Furthermore, shorter light exposure times did not lead to comparable activation of cells relative to the positive agonist control. This was due to incomplete deprotection of **2**.

We confirmed that UV light did not have an effect on cells. We compared NF-κB activity in cells treated with media only, with and without UV light. Additionally, we tested treatment with **2** and directly exposed to light versus cells treated with a pre-irradiated solution of **2**. Direct UV light exposure for the time employed did not affect cell activity (**Figure 2.10**). It is important to note that longer light exposure times, different or more intense light sources, or more sensitive cells may lead to cell activation, damage, or death.

Treatment of RAW-Blue cells with **2** without UV light resulted in minimal NF-κB activity. This background activity is likely due to enzymatic activity over the time course of the experiment. To confirm that enzymatic degradation was producing active agonist, **2** was incubated in culture conditions (acellular) with and without serum proteins. Following overnight incubation, the samples were analyzed by LCMS. Only one major peak with a mass of 640 ($M_{\text{caged agonist}}+1$) was

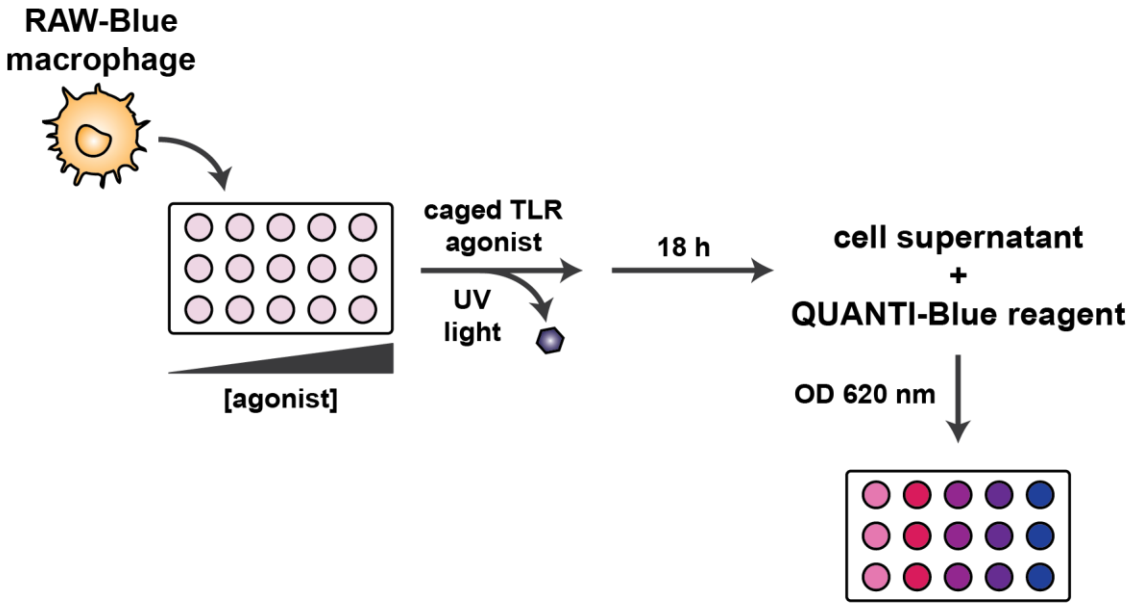

Figure 2.8. Scheme of light-controlled NF-κB activation in reporter cells, RAW-Blue macrophages. Cells were plated in 96-well plates and treated with unmodified or caged agonist and exposed to UV light (365 nm). After overnight incubation, SEAP levels are determined by a colormetric assay, whereby the cell supernatant is treated with QUANTI-Blue reagent.

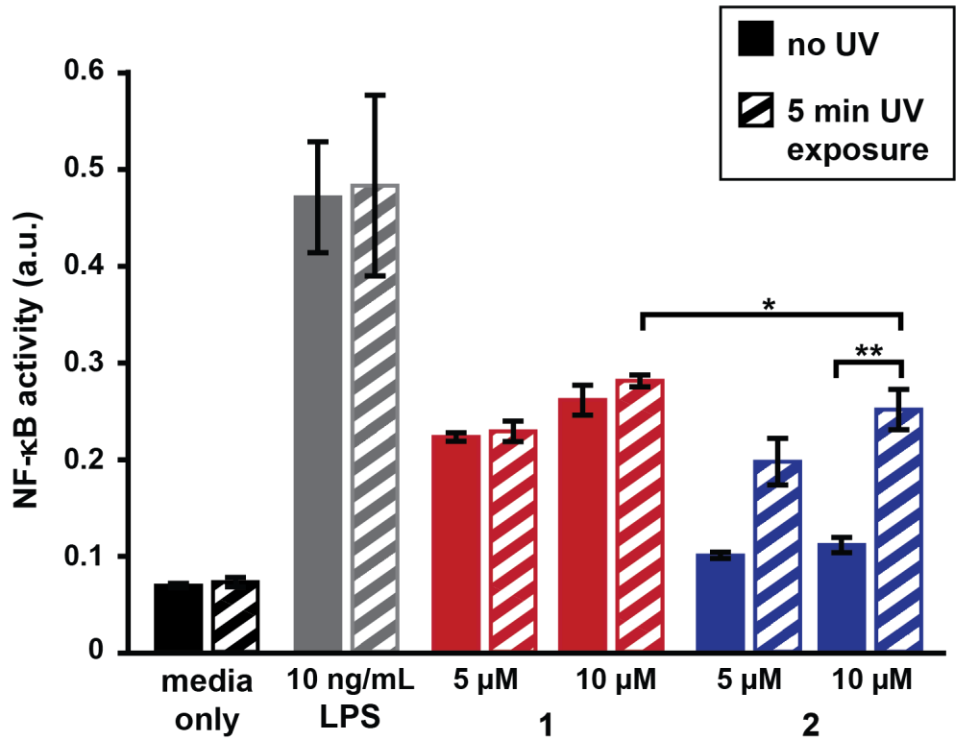

Figure 2.9. Light-controlled NF-κB activation in reporter cells, RAW-Blue macrophages. Caged agonist **2** does not activate TLR4 until photo-controlled deprotection with UV light to produce the active TLR4 agonist **1**. Cells were treated with media only (black), LPS (10 ng/mL; gray), **1** (10 μM; red), **2** (10 μM; solid blue), without (solid) or with (outlined) UV light exposure (15W, 365 nm light). NF-κB activation was determined using the SEAP colorimetric assay (OD measured at 620 nm). Each experiment was performed in replicates of five (*$p < 0.05$ and **$p < 0.001$).

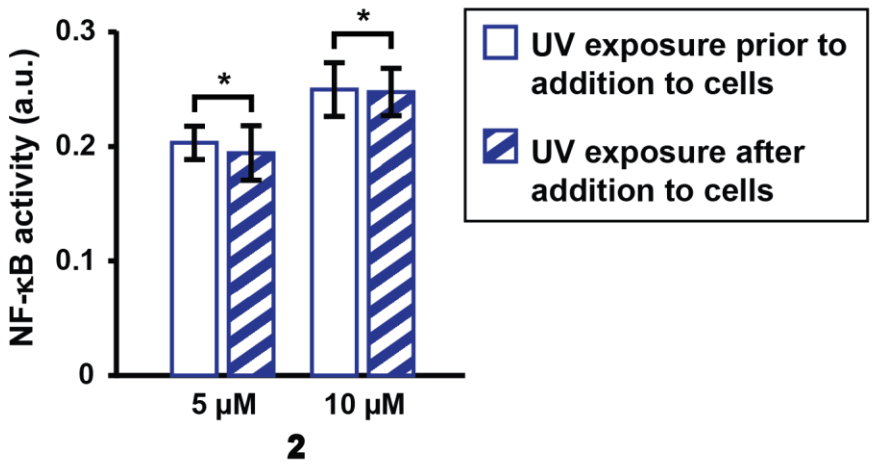

Figure 2.10. Effect of UV light exposure on light-controlled NF-κB activation in reporter cells. RAW-Blue macrophages were treated with **2** (5 and 10 μM) with UV light exposure prior to addition of cells (solid white), or in the presence of cells (striped). NF-κB activation was measured by taking the OD at 620 nm. Each experiment was performed in replicates of five (*$p < 0.05$).

detected in samples treated with serum-free media. Conversely, two peaks of masses 433 ($M_{agonist}$+1) and 640 were detected in samples exposed to serum proteins. We confirmed that the carbamate linkage between the indole and the protecting group is also enzymatically labile within the long time course of the RAW-Blue cell experiments. Enzymatic cleavage, however, does not pose an issue in studies probing spatial and temporal activation, as these factors are of importance in the minute's to hours' time frame. The accumulation of deprotected, active agonist caused my enzymatic cleavage is insignificant and would not contribute to background activation. Furthermore, as discussed in the next section, we did not observe background activation in experiments that probe real time activation of TLR4.

Real-time immune activation

Activation of TLR4 *via* light was performed in a second reporter cell line - 3T3 fibroblasts expressing p65-DsRed. NF-κB activation was observed in real time *via* optical microscopy in a dose-dependent study using the caged agonist. Here, NF-κB activity is defined as the nuclear translocation of NF-κB as measured by the subunit of NF-κB, p65, that is fluorescently labeled - p65-DsRed.[27,28] This nuclear translocation was observed by confocal microscopy and quantified using ImageJ analysis. The discrimination between nucleus and cytoplasm for these experiments is afforded by a second fluorescent protein expressed by the cell, H2B-GFP, which is a histone protein and is only found in the nucleus.

Fibroblasts were treated with TLR4 agonist **1** or caged agonist **2** (0.625-5.0 μM) at t=0 and images were recorded for 3 h (**Figure 2.11-2.12**). NF-κB translocation was observed in cells treated with **1**. When stimulated with **1**, the peak translocation of NF-κB occurs after 45 min. Translocation was not observed at any time point measured in cells treated with media only or the

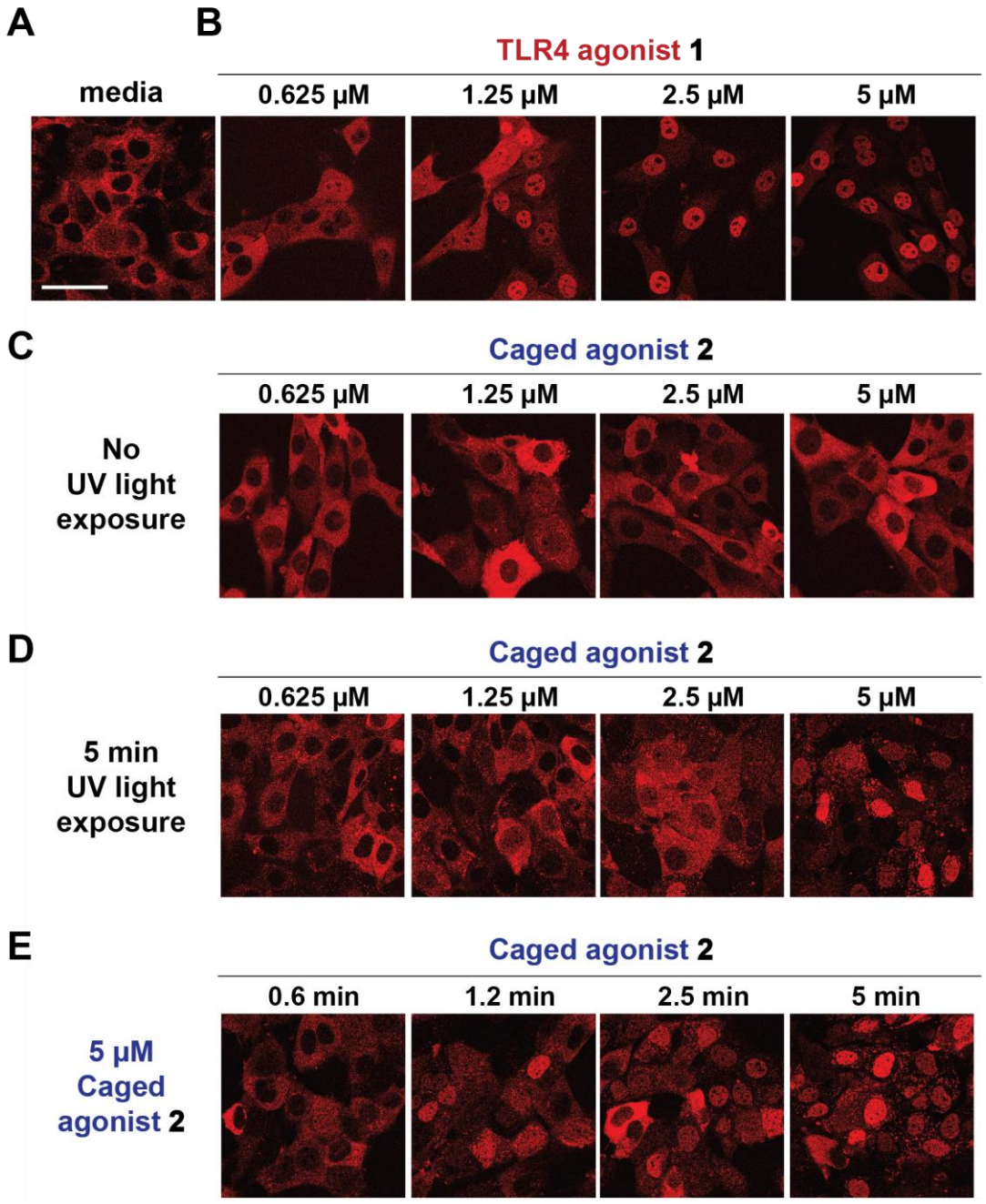

Figure 2.11. Light-controlled NF-κB activation in fluorescent NF-κB reporter cells. Confocal images of p65-DsRed fibroblasts 45 min after treatment with media only (**A**), TLR4 agonist **1** (**B**), caged agonist **2** (**C**), caged agonist with 5 min bulk UV light exposure (**D**), and 5 μM of caged agonist **2** exposed to UV light for times ranging from 0.6 to 5 min (**E**). The scale bar is equal to 50 μm.

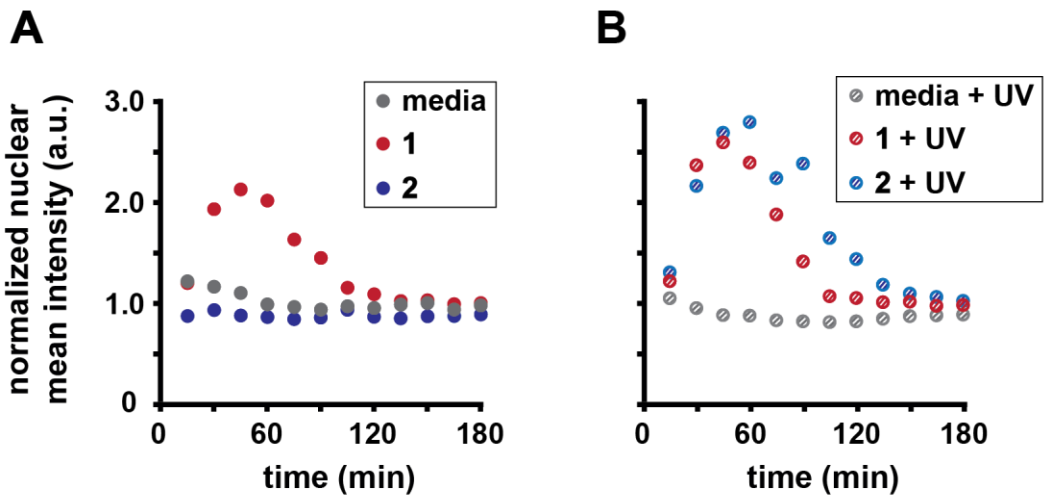

Figure 2.12. Quantification of NF-κB activation in fluorescent reporter cells. The red nuclear intensity was determined by ImageJ analysis for cells treated with media, **1** or **2**, without and with 5 min light exposure (15 W, 365 nm). See **Appendix B** for confocal images.

equivalent concentrations of caged agonist, **2**, without UV light exposure. The dose-dependent trend in activation seen with **1** was reestablished by treating cells with varying concentrations of **2** followed by 5 min UV light exposure (15 W, 365 nm). To further confirm that activation was dependent on light, cells were treated with **2** at a fixed concentration and UV light exposure time was varied (0.6-5 min). When cells are treated in this manner, the degree of translocation is observed to be a function of exposure time. In cells treated with **2** and exposed to UV light, the maximal translocation of p65-DsRed occurred at 45 min, the same time as with treatment of **1**.

Spatially-controlled immune activation

To date, our understanding of the immune system is based on bulk methods of activation. Work described in a later section focused on immune responses of heterogeneous co-cultures and how activation of a cell subset impacts the bulk response.[29] With our light-controlled TLR4 agonist, we sought to address the minimum requirements for immune activation at the population level. Here, we aimed to exert spatial control over immune activation by limiting agonist exposure to a subpopulation of cells using light. Spatial control was implemented using two methods: by light exposure through a pinhole mask (**Figure 2.13**) and two-photon confocal microscopy. In using this method to activate cells, factors involving the cells, agonist, and light are all important. These factors include cell density over the culture area, cell media composition, agonist concentration, light exposure time and area, and the wavelength and power of the light. We predicted that exposure time in these experiments would play a critical role. We expected that under exposure would not produce a high enough local concentration of agonist to activate cells; conversely, over exposure would produce too high of an agonist concentration across the culture that could activate more than the desired subpopulation. Both of these results are possible because

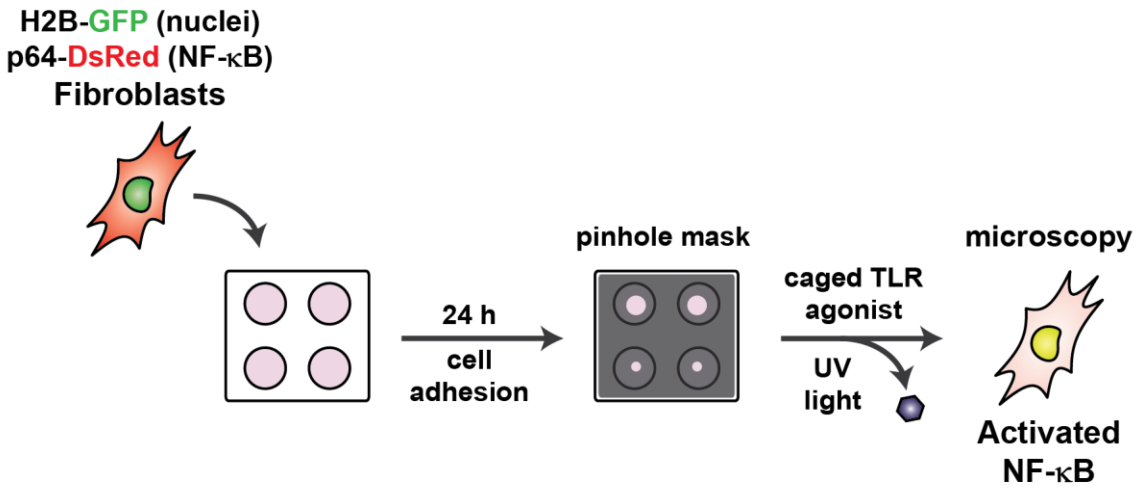

Figure 2.13. Scheme of light-controlled NF-κB activation in fluorescent reporter cells, p65-DsRed fibroblasts. Cells were plated in coverslip-bottomed 8-well plates and treated with caged agonist **2** and exposed to UV light (365 nm). Following light exposure, the pinhole mask was removed and cells were imaged by confocal microscopy.

of the rapid diffusion of molecules in and out of the region of interest (diffusion of a small molecule in water is ~10^{-5} cm^2/s).

The first attempt at spatially-controlled deprotection and resulting activation of cells was performed using the pinhole mask method using the same UV lamp source (15 W, 365 nm) as used in the initial experiments with RAW-Blue cells. Fibroblasts expressing p65-DsRed were treated with **2** (10 μM) and spatial control was implemented by light exposure through a pinhole mask (3.1 mm^2 exposure area in a 80.1 mm^2 well). The exposure area resulted in the direct exposure of some 200 cells for the cell density used in these experiments. Here, NF-κB translocation occurred in cells within the pinhole area, and the degree to which activation occurs tapered as a function of distance from the pinhole (**Figure 2.14-2.15**). To be expected, cells adjacent to the light-exposed area (x-coordinate of 2000-2500 μm) would exhibit similar levels of NF-κB translocation because of rapid diffusion of the active agonist. To achieve this result, the light exposure time was longer than in the bulk deprotection experiments (15 min compared to 5 min). This difference confirmed our hypothesis regarding the diffusion of the active agonist.

Ongoing research in our group focuses on using the techniques developed herein to afford controlled activation, down to the single cell level, for which these initial results are the first step. Smaller regions of interest are selectable using our light-based method, however, we did not observe translocation using smaller pinholes for light exposure. Potential reasons for this finding include low local concentrations of the agonist, low light source power, and/or non-optimal light source wavelength (lamp λ_{max} = 365 nm; NVOC λ_{max} = 340 nm). Other attempts to improve deprotection and achieve selective activation over a small number of cells using the pinhole mask method, including using higher concentrations of **2** (20 μM or greater) or longer exposure times

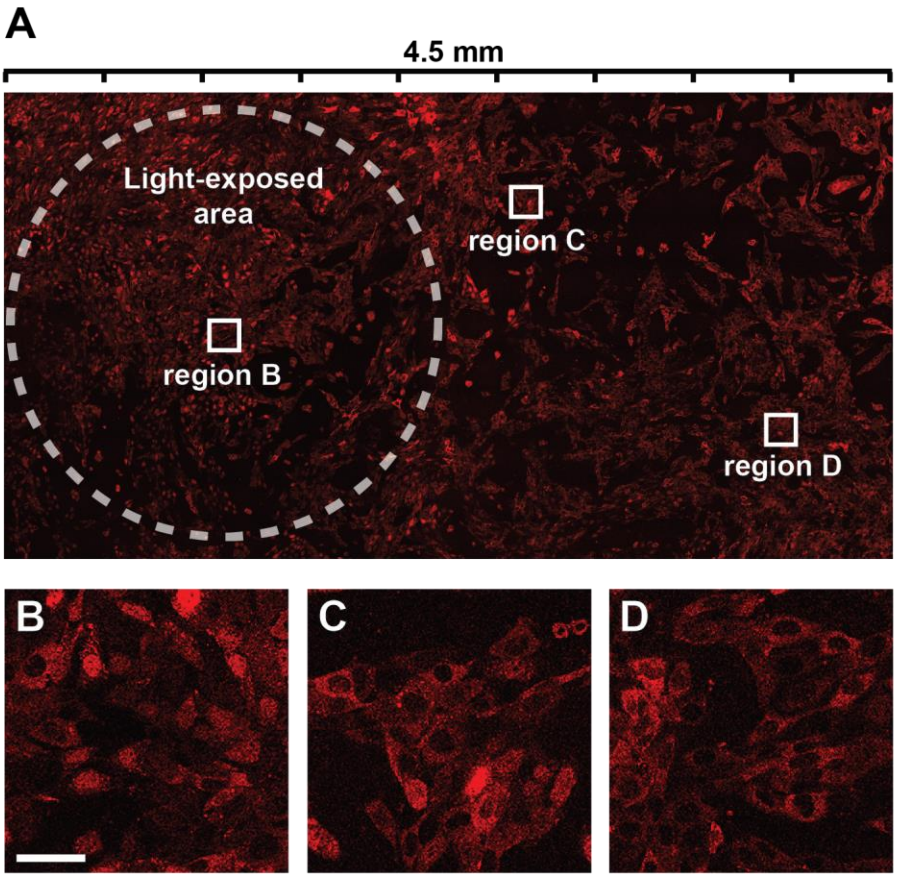

Figure 2.14. Light-controlled NF-κB activation in fluorescent NF-κB reporter cells. Confocal images of p65-DsRed fibroblasts 45 min after treatment with caged agonist **2** and 15 min UV light exposure through a pinhole mask. Light exposure was confined to a 3.1 mm^2 pinhole (dashed white line, **A**). Cells within the exposed pinhole (**B**) show high degrees of NF-κB translocation, while cells further from the pinhole (**C** and **D**) have less. The scale bar is equal to 50 μm.

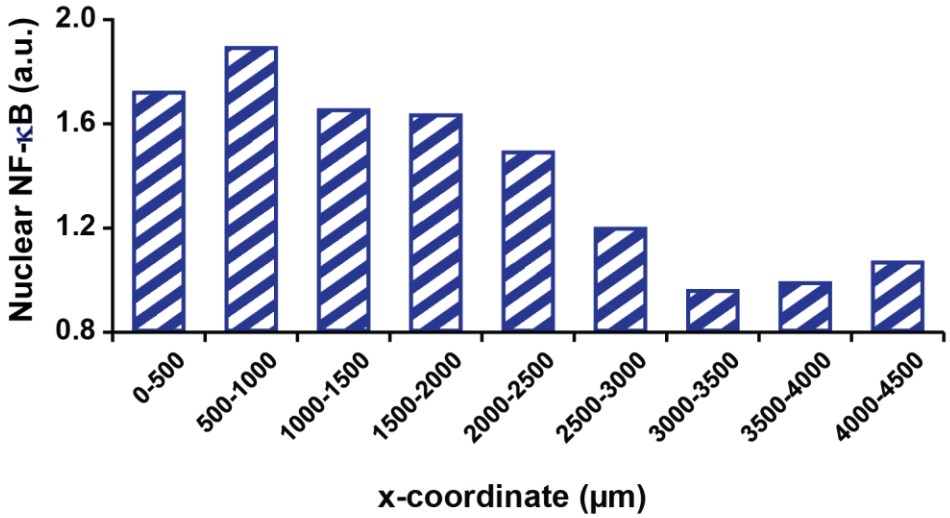

Figure 2.15. Light-controlled NF-κB activation in fluorescent NF-κB reporter cells. Confocal images of p65-DsRed fibroblasts were taken follow selective light exposure. Quantification of translocation of the fluorescent transcription factor was performed using ImageJ analysis (see **Appendix A-B** for image acquisition and quantification protocol).

(20 min or more), resulted in cell damage and death due to toxicity of high agonist concentrations and over-exposure to UV light.

We employed confocal microscopy to optimally deprotect the caged agonist and observe in real time the activation of small clusters of cells. Specifically, two-photon excitation was used to uncage **2** at a wavelength nearer to the λ_{max} of NVOC. The variables of two-photon excitation are numerous, including laser power, number of scans, and residence time. Additionally, the exposure area can be digitally selected on the microscope computer setup, affording us greater spatial control of the light. Here, the two-photon exposure area spanned the area of ~10-20 cells. The light source was set to the lowest possible two-photon setting of 710 nm. This meant that cells in the focal plane would be exposed to light of 710/2 nm = 355 nm. Fibroblasts expressing p65-DsRed were treated with **2** (10 μM) and immediately subjected to the light exposure. Preliminary results showed that we were able to achieve some translocation of NF-κB in cells surrounding an exposure area (**Figure 2.16**). Cells directly in the light path, however, were observed to die and separate from the culture surface. This immediate cell death observed was due to the cells experiencing an intense, focused flash of light that likely superheated the solution surrounding the cells, leading to damage. Studies performed treating cells only with light and no agonist gave this result. Working continuing in the group focuses on finding the balance between light intensity and total exposure time to yield the desired localized activation of cells.

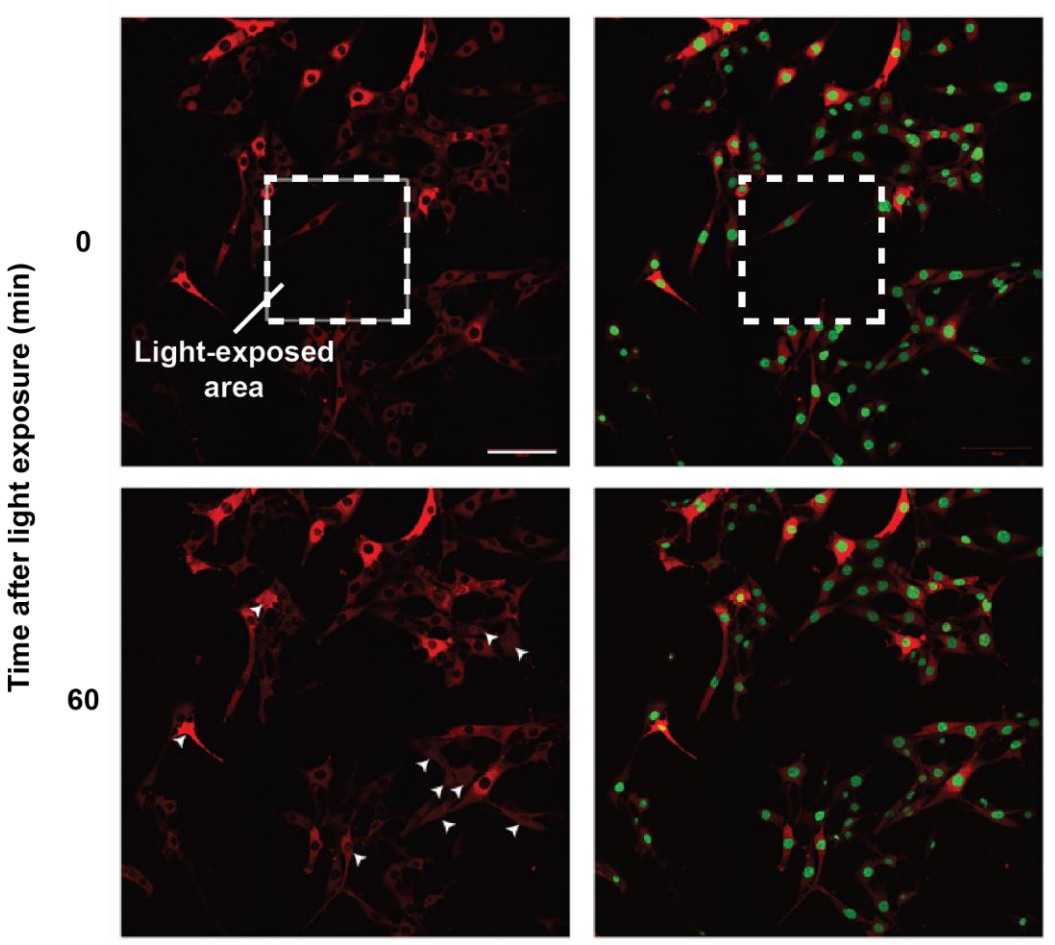

Figure 2.16. Light-controlled NF-κB activation in fluorescent NF-κB reporter cells. Confocal images of p65-DsRed fibroblasts 45 min after treatment with caged agonist **2** and UV light exposure using the two-photon deprotection method. Light exposure was confined to a 0.04 mm^2 pinhole (dashed white line). Cells surrounding the light-exposed area showed NF-κB translocation 60 min after light exposure (activated cells are indicated with white arrows). The scale bar is equal to 10 μm.

Summary of spatially-controlled immune activation using a caged TLR4 agonist

Here we show the synthesis of a photo-controlled TLR4 agonist and a method that controls spatial activation of innate immune cells. Protection of the critical indole nitrogen of pyrimido[5,4-*b*]indole with a photo-labile group reduced TLR activity to background levels. Upon exposure to UV light, compound **1** was regenerated, which then activated NF-κB signaling pathways via TLR4. We showed activation of innate immune cells, RAW macrophages, is mediated by UV light exposure of the caged agonist. Furthermore, we demonstrate for the first time the selective activation of a subpopulation of cells (~200 cells) within a larger population (1000's of cells) by confining light exposure of the caged agonist through a pinhole. Preliminary results have been obtained for the selective activation of smaller clusters of cells (<20 cells) using two-photon confocal microscopy.

With this and similar tools, we plan to explore how immune activation propagates from an origin of inflammation, as well as how TLR synergies can be modulated both spatially and temporally. We aim to understand how TLR signaling contributes at different levels to both positive and deleterious immune responses.

References

(1) Ohto, U.; Fukase, K.; Miyake, K.; Shimizu, T. *Proc. Natl. Acad. Sci.* **2012**, *109* (19), 7421–7426.
(2) Park, B. S.; Song, D. H.; Kim, H. M.; Choi, B.-S.; Lee, H.; Lee, J.-O. *Nature* **2009**, *458* (7242), 1191–1195.
(3) Stover, A. G. *J. Biol. Chem.* **2003**, *279* (6), 4440–4449.
(4) Coler, R. N.; Baldwin, S. L.; Shaverdian, N.; Bertholet, S.; Reed, S. J.; Raman, V. S.; Lu, X.; DeVos, J.; Hancock, K.; Katz, J. M.; Vedvick, T. S.; Duthie, M. S.; Clegg, C. H.; Van Hoeven, N.; Reed, S. G. *PLoS ONE* **2010**, *5* (10), e13677.
(5) Coler, R. N.; Bertholet, S.; Moutaftsi, M.; Guderian, J. A.; Windish, H. P.; Baldwin, S. L.; Laughlin, E. M.; Duthie, M. S.; Fox, C. B.; Carter, D.; Friede, M.; Vedvick, T. S.; Reed, S. G. *PLoS ONE* **2011**, *6* (1), e16333.
(6) O'Neill, L. A. J.; Golenbock, D.; Bowie, A. G. *Nat. Rev. Immunol.* **2013**, *13* (6), 453–460.
(7) Trompette, A.; Divanovic, S.; Visintin, A.; Blanchard, C.; Hegde, R. S.; Madan, R.; Thorne, P. S.; Wills-Karp, M.; Gioannini, T. L.; Weiss, J. P.; Karp, C. L. *Nature* **2008**, *457* (7229), 585–588.
(8) Bryant, C. E.; Spring, D. R.; Gangloff, M.; Gay, N. J. *Nat. Rev. Microbiol.* **2009**.
(9) Shanmugam, A.; Rajoria, S.; George, A. L.; Mittelman, A.; Suriano, R.; Tiwari, R. K. *PLoS ONE* **2012**, *7* (2), e30839.
(10) Ohashi, K.; Burkart, V.; Flohé, S.; Kolb, H. *J Immunol* **2000**, *164*, 558.
(11) Asea, A.; Rehli, M.; Kabingu, E.; Boch, J. A.; Baré, O.; Auron, P. E.; Stevenson, M. A.; Calderwood, S. K. *J. Biol. Chem.* **2002**, *277* (17), 15028–15034.
(12) Smiley, S. T.; King, J. A.; Hancock, W. W. *J Immunol* **2001**, *167*, 2887.
(13) Okamura, Y.; Watari, M.; Jerud, E. S.; Young, D. W.; Ishizaka, S. T.; Rose, J.; Chow, J. C.; Stauss III, J. F. *J. Biol. Chem.* **2001**, *276* (13), 10229–10233.
(14) Semeraro, F.; Ammollo, C. T.; Morrissey, J. H.; Dale, G. L.; Friese, P.; Esmon, N. L.; Esmon, C. T. *Blood* **2011**, *118* (7), 1952–1961.
(15) Chan, M.; Hayashi, T.; Mathewson, R. D.; Nour, A.; Hayashi, Y.; Yao, S.; Tawatao, R. I.; Crain, B.; Tsigelny, I. F.; Kouznetsova, V. L.; Messer, K.; Pu, M.; Corr, M.; Carson, D. A.; Cottam, H. B. *J. Med. Chem.* **2013**, *56* (11), 4206–4223.
(16) Nour, A.; Hayashi, T.; Chan, M.; Yao, S.; Tawatao, R. I.; Crain, B.; Tsigelny, I. F.; Kouznetsova, V. L.; Ahmadiiveli, A.; Messer, K.; Pu, M.; Corr, M.; Carson, D. A.; Cottam, H. B. *Bioorg. Med. Chem. Lett.* **2014**, *24* (21), 4931–4938.
(17) Mata-Haro, V.; Cekic, C.; Martin, M.; Chilton, P. M.; Casella, C. R.; Mitchell, T. C. *Science* **2007**, *316* (5831), 1628–1632.
(18) Gangloff, M. *Trends Biochem. Sci.* **2012**, *37* (3), 92–98.
(19) Bowen, W. S.; Minns, L. A.; Johnson, D. A.; Mitchell, T. C.; Hutton, M. M.; Evans, J. T. *Sci. Signal.* **2012**, *5* (211), ra13–ra13.
(20) Mata-Haro, V.; Cekic, C.; Martin, M.; Chilton, P. M.; Casella, C. R.; Mitchell, T. C. *Science* **2007**, *316* (5831), 1628–1632.
(21) Mancini, R. J.; Stutts, L.; Ryu, K. A.; Tom, J. K.; Esser-Kahn, A. P. *ACS Chem. Biol.* **2014**, *9* (5), 1075–1085.
(22) Sung, M.-H.; Li, N.; Lao, Q.; Gottschalk, R. A.; Hager, G. L.; Fraser, I. D. C. *Sci. Signal.* **2014**, *7* (308), ra6–ra6.

(23) Napolitani, G.; Rinaldi, A.; Bertoni, F.; Sallusto, F.; Lanzavecchia, A. *Nat. Immunol.* **2005**, *6* (8), 769–776.
(24) Hemphill, J.; Chou, C.; Chin, J. W.; Deiters, A. *J. Am. Chem. Soc.* **2013**, *135* (36), 13433–13439.
(25) Mancini, R. J.; Tom, J. K.; Esser-Kahn, A. P. *Angew. Chem. Int. Ed Engl.* **2014**, *53* (1), 189–192.
(26) Govan, J. M.; Young, D. D.; Lively, M. O.; Deiters, A. *Tetrahedron Lett.* **2015**.
(27) Ashall, L.; Horton, C. A.; Nelson, D. E.; Paszek, P.; Harper, C. V.; Sillitoe, K.; Ryan, S.; Spiller, D. G.; Unitt, J. F.; Broomhead, D. S.; Kell, D. B.; Rand, D. A.; See, V.; White, M. R. H. *Science* **2009**, *324* (5924), 242–246.
(28) Tay, S.; Hughey, J. J.; Lee, T. K.; Lipniacki, T.; Quake, S. R.; Covert, M. W. *Nature* **2010**, *466* (7303), 267–271.
(29) Mancini, R. J.; Stutts, L.; Moore, T.; Esser-Kahn, A. P. *Angew. Chem. Int. Ed.* **2015**, *54* (20), 5962–5965.

CHAPTER 3: Light-controlled agonists for TLR7 and 8 and progress towards TLR4-7,8 synergy studies

Overview of TLR7,8 signaling

Receptor structure and agonists

Toll-like Receptors 7 and 8 are related PRRs that mediate responses to viral pathogen ligands. TLR7 and TLR 8 detect single-stranded RNA (ssRNA), as well as nucleoside-like small molecules, including imidazoquinoline, thiazoquinoline, and benzoazepine derivatives.[1–3] Some of these small molecule activators, imiquimod (R837) and resiquimod (R848) are used in topical treatment of tumors. Like other TLRs, TLR7 and 8 are membrane-bound, horseshoe-shaped receptors that have leucine-rich repeat (LRR) regions and Toll-Interleukin-1-Resistance (TIR) domains. The unique aspect of these receptors is that they exist as a homodimer prior to ligand recognition and activation. The crystal structure of TLR8 indicates that prior to agonist binding, the C-terminal domains of the dimer pair are 53 Å apart, a distance that prevents association of the TIR domains (**Figure 3.1**).[4–6] Upon agonist binding, the subunits undergo a conformational shift, which brings the C-terminal domains to 23 Å apart to afford dimerization of the TIR domains. This event allows for the interaction of the TLR complex to the signaling protein MyD88.

Single-stranded RNAs induce an interferon response in dendritic cells through TLRs. Specifically, polyuridylic acid and other U-rich strands are the most active ssRNAs.[1] The binding mode of ssRNAs with these receptors has not been characterized, and much of what we know about these receptors and the progress towards developing disease treatments and vaccines has been achieved through use of the small molecule immunostimulants (**Figure 3.2**). The imidazoquinoline family of agonists are potent and have been derivatized for many applications.

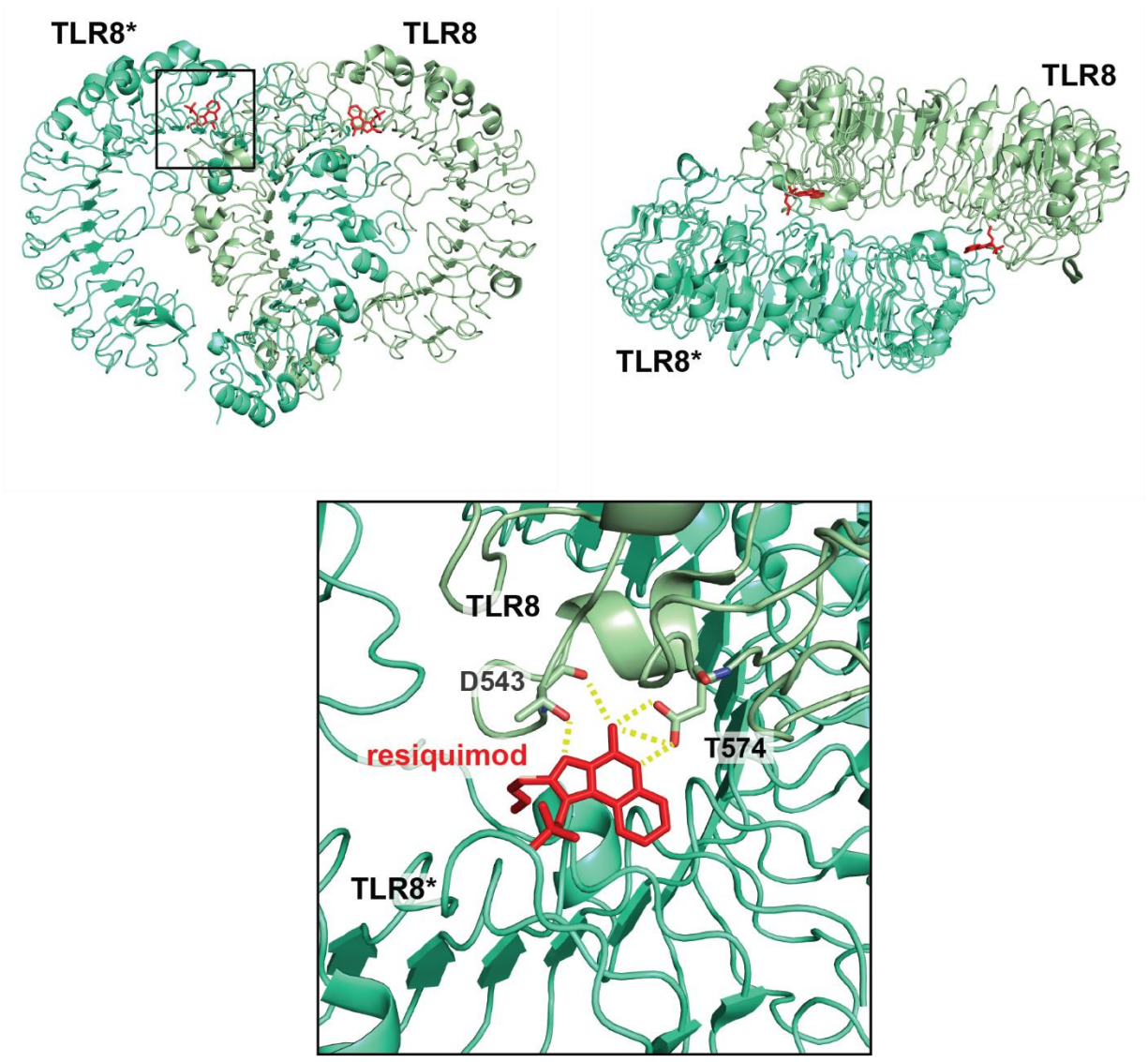

Figure 3.1. Crystal structure of TLR8 with resiquimod. Imidazoquinoline agonist associate with binding pockets at the receptor dimer interface, but the primary interactions occur via hydrogen bonding with the D543 and T574 residue of one receptor.

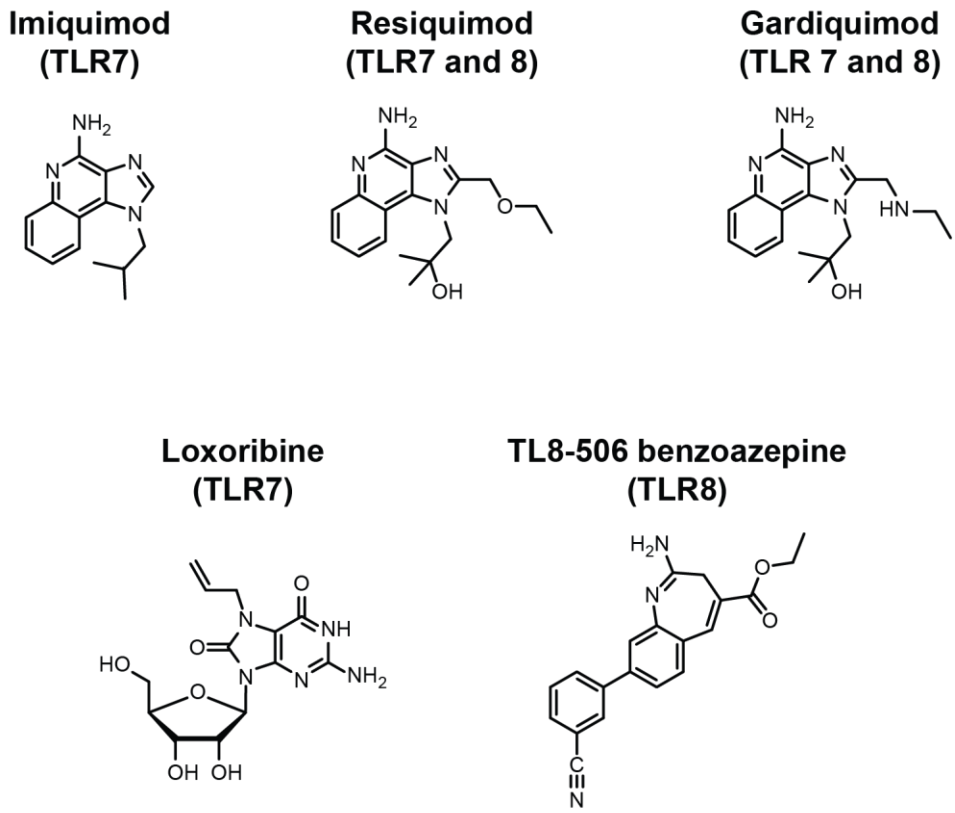

Figure 3.2. Common TLR7 and 8 agonists. Imidazoquinoles, imiquimod, resiquimod, and gardiquimod, and others have specificity of TLR7 or 8 binding and activation.

The TLR7 agonist 9-benzyl-8-hydroxy-2-(2-methoxyethoxy) adenine was modified for conjugation to a phospholipid, PEG, and phospholipid-PEG via the benzoic acid functional group of the agonist.[7] The conjugates with 18-unit or longer PEG chains showed improved agonistic activity. Phospholipid conjugation enhanced activity over 100-fold relative to the unmodified agonist.[8] Modifications to a TLR8 agonist, thiazolo[4,5-c]quinoline prove that alkyl chains at the C2 position of up to 3 carbons increase potency, while alkylation of any kind at C4 was not tolerated.[9] Dimeric and dendritic agonists of imidazoquinolines linked at C4, C8, and N1-aryl positions have also been synthesized and activate via TLR7 and 8.[10] Dendrimers linked at N1-aryl positions had greater potency than the single, unmodified agonist. These findings imply that spatial factors in the nano- and microscale are of consequence in immune activation.

TLR7 and 8 signaling

TLR7 and 8 are endosomal receptors that signal through the MyD88 pathway (**Figure 3.3**). The transcriptional outcomes of the endosomal MyD88 pathway are simultaneous activation of NF-κB, AP1, and CREB, as well as Interferon Regulating Factor 7 (IRF7). The former three activators elicit a pro-inflammatory response, while IRF7 elicits a viral response through Type I interferons.

Probing TLR7 and 8 activation mechanisms

Similar to work described in an earlier section, the goal of this research was to study the spatial and temporal contributions of TLR activation using a light-controlled agonist. We strategically chose to generate controllable TLR7 and 8 agonists alongside the caged TLR4 agonists because these receptors, or pathways they individually activate, have been identified as

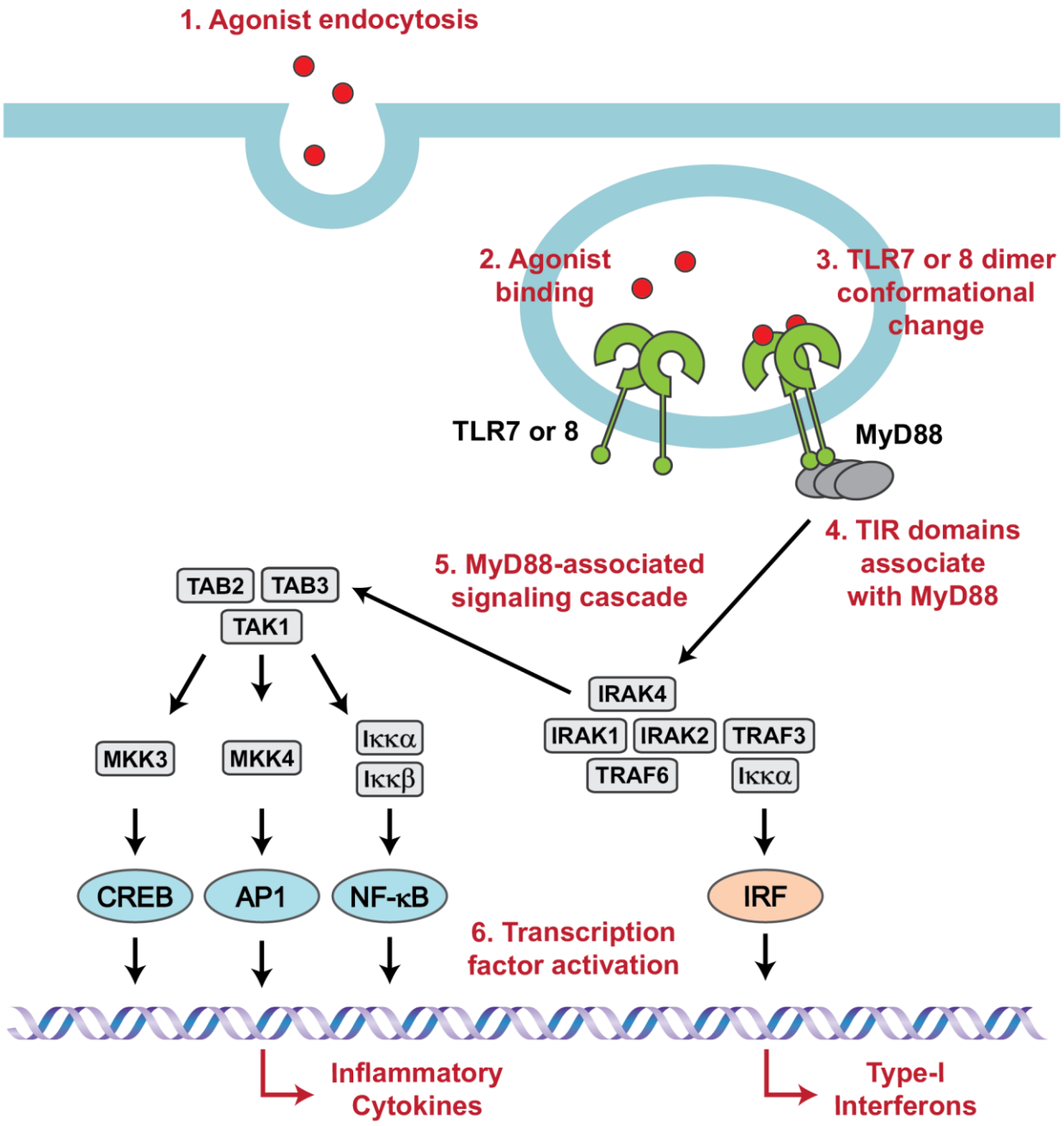

Figure 3.3. TLR7 and 8 signaling pathways. Activation of endosomal TLR7 and 8 results in signaling of the MyD88 pathway. This pathway leads to activation of both inflammatory cytokines and interferons.

strong synergistic pairing.[11]

Again, manipulation of the agonist was achieved by protection with a photo-labile protecting group at a position on the agonist critical for receptor interaction. The compound, when protected, would be unable to activate the receptor; however, upon deprotection with light, the agonist will induce the dimer conformational change and initiate the signaling cascade. The goal of this work was to create the first controllable TLR7 and 8 agonists and apply them in experiments with the orthogonal light-controlled TLR4 agonist.

Here, two imidazoquinoline agonists were chosen for protection and light-activation: imiquimod (R837, **3**) and resiquimod (R848, **4**; **Figure 3.4**). In addition to being commonly used immunostimulants, these small molecules are synthetically less challenging than the native ssRNA targets of TLR7 and 8. Additionally, SAR studies with both TLR7 and 8 agonists and crystallographic data have identified residues critical for activity. The aromatic rings of imidazoquinolines stack with Phe residues on both TLR8s of the dimer. Alkyl and/or ether chains attached to the imidazoquinoline can protrude into a hydrophobic pocket. Within the binding pocket of TLR8, Asp543, is essential for ligand recognition, and the C4 amine of imidazoquinolines has been shown to play a critical role in binding to D543 and T574 positions (**Figure 3.1**).[6,12] Modification of imiquimod and resiquimod C4 amines would, therefore, interrupt agonist-receptor binding and conformational change. In this work, we chose to install the photo-labile cage, 2-(2-nitrophenyl)propyloxycarbonyl (NPPOC). This protecting group is labile to UV light (NPPOC λ_{max} = 365 nm). Light-controlled activation of TLR7 and 8 was assessed using a NF-κB reporter cell line, RAW-Blue macrophages.

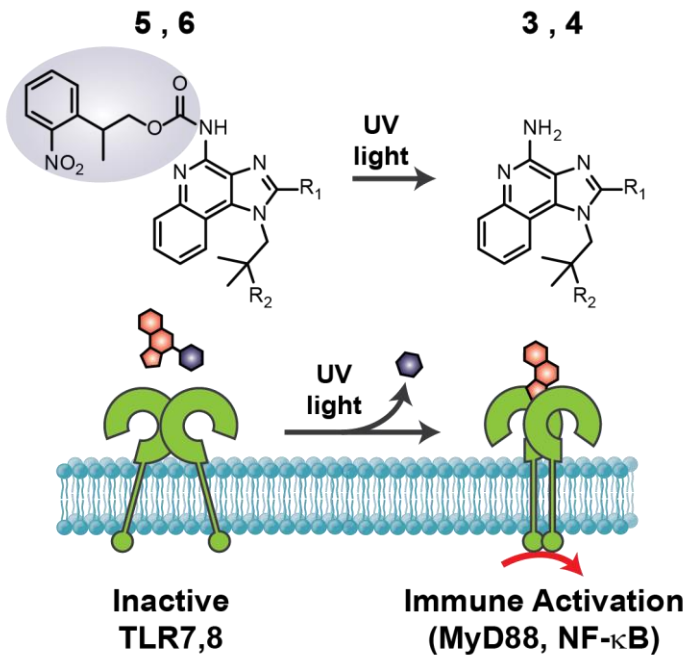

Figure 3.4. Photo-controlled deprotection of caged TLR7 and 8 agonists. NPPOC-caged imiquimod **5** and resiquimod **6** is converted to **3** and **4**, respectively, using UV light (365 nm) to activate immune cells via TLR7 or 8. Imiquimod (R_1 = H, R_2 = H). Resiquimod (R_1 = -$CH_2OCH_2CH_3$, R_1 = OH).

Design and characterization of caged TLR7 and 8 agonists

Synthesis of the TLR7 and 8 caged agonists

The synthesis and characterization of caged imiquimod **5** and caged resiquimod **6** was performed by Keun Ah Ryu. Briefly, imiquimod (30 mg, 0.2 mmol) was stirred in anhydrous 1,4 dioxane at 10 °C. 2-(2-nitrophenyl)propyloxycarbonyl chloride (NPPOC-Cl, 61 mg, 0.4 mmol) in anhydrous 1, 4 dioxane was added dropwise to the agonist solution. The reaction mixture was heated to 50 °C for 6 hr. The solution was concentrated under vacuum and purified by silica gel column chromatography to obtain **5** (38 % yield). Similarly, resiquimod (30 mg, 0.1 mmol) was stirred in anhydrous 1,4 dioxane at 10 °C. NPPOC-Cl (47 mg, 0.2 mmol) was diluted in anhydrous 1, 4 dioxane and added dropwise to the agonist solution. The reaction mixture was heated to 50 °C for 6 hr. The solution was concentrated under vacuum and purified by silica gel column chromatography to obtain **6** (16 % yield). Protection of the C4 nitrogen for both imiquimod and resiquimod was confirmed *via* high-resolution mass spectrometry, and ^{1}H and ^{13}C NMR spectroscopy.[13]

Activation of cells using light

Preliminary assessment of immune activation

We confirmed that photo-deprotection of the caged agonist translated to light-controlled activation of TLR7 and 8 by testing **5** and **6** on a model cell line bearing TLRs—RAW-Blue macrophages. These cells express TLRs, including TLR7 and 8, and a secreted embryonic alkaline phosphatase (SEAP) reporter for NF-κB activation (**Figure 2.8**). SEAP levels are monitored using a detection medium, QUANTI-Blue, affording a colorimetric readout of TLR activation. This assay served as an initial examination of immune activity of the unmodified **3** and **4** and caged **5**

and **6** agonists. Based on the previous SAR study of **3** and **4**[14] and crystallography data of **4** with TLR8, we predicted that **5** and **6** after UV light exposure, would affect immune activity, while **5** and **6** without UV light exposure, would have little to no effect on NF-κB activity in cells.

RAW-Blue cells were treated with **3**, **4**, **5** and **6** (2 and 20 μM), then exposed to UV light (4 W, 365 nm) for 20 min. The light exposure times here differ from those discussed in light-controlled TLR4 activation, as the power of the UV light sources were different. The cells were incubated for 18 h before the culture supernatant was analyzed to determine NF-κB activation. We observed the selective activation of cells upon UV light exposure (**Figure 3.5**). Treatment with **5** and **6** with exposure to UV light yielded NF-κB activity equivalent in concentration to the corresponding parent agonists. Treatment of RAW-Blue cells with **X** without UV light resulted in non-significant NF-κB activity relative to cells treated with media only.

Real-time immune activation

Activation of TLR7 via light was performed in bone marrow-derived dendritic cells (BMDCs). These are primary cells obtained from mice, and are considered more relevant in assessing immune activation. In these experiments, we measured activation via endocytosis, rather than a single pathway or cytokine. Dendritic cells constantly undergo endocytosis and phagocytosis as a method of surveying their surroundings and detecting pathogens. Upon initiation of immune pathways, such as NF-κB, the cells speed up this process to enhance pathogen update and antigen presentation.[15] This stage of dendritic cell maturation can be visualized using microscopy within 15 minutes of TLR ligand exposure. As a reference, translocation of NF-κB occurs after 30-45 min after stimulation, and generally cytokine analysis occurs hours after.

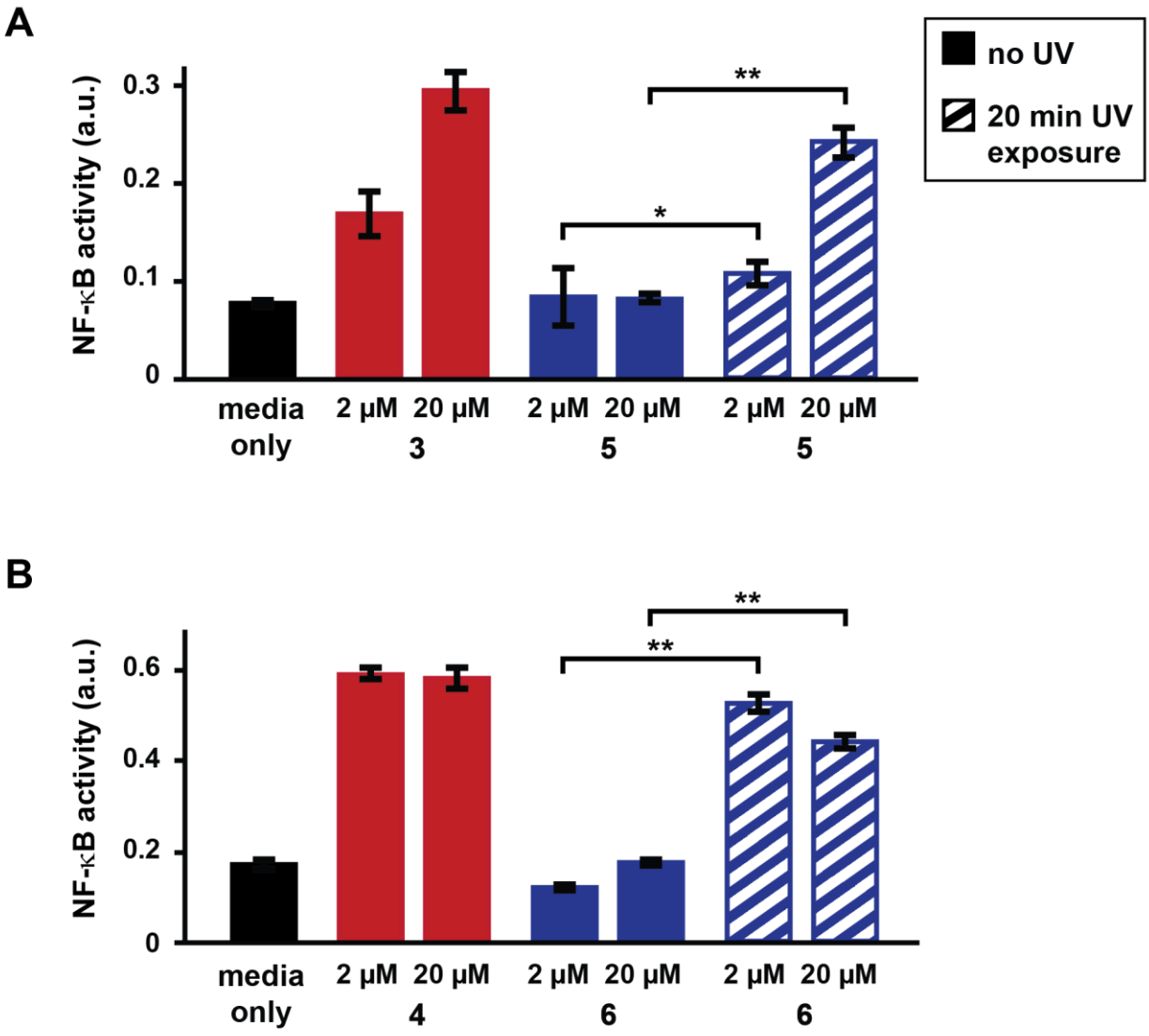

Figure 3.5. Light-controlled NF-κB activation in reporter cells, RAW-Blue macrophages. Caged agonists **5** and **6** do not activate cells until photo-controlled deprotection with UV light to produce the active agonists **3** and **4**, respectively. Cells were treated with media only (black), **5** (2 or 20 μM; red), **3** (2 or 20 μM; solid blue), without (solid) or with (outlined) UV light exposure (4W, 365 nm light, **A**). NF-κB activation was determined using the SEAP colorimetric assay (OD measured at 620 nm). Each experiment was performed in replicates of five (*$p < 0.047$ and **$p < 0.0001$).

To observe activation of BMDCs in real time, cells were treated with a fluorescently-labeled dextran along with the agonist (**Figure 3.6**). We hypothesized that cells treated with the active agonists **4** and those treated with **6** with UV exposure would show rapid endocytosis compared to the control samples, media only or **6** without UV exposure. We expected that some amount of endocytosis would be observed in the control samples, as the process occurs to some extent in quiescent cells. Cultures were imaged before and for 1-2 hr after treatment. We first observed that cells treated with media only did show a low level of endocytosis, 0-5 endosomes per cell (**Figure 3.7**). In samples treated with **4** and **6** with UV light, cells appeared to become stimulated within 15-30 min. In addition to increased number of endosomes, 10 or more per cell, changes in cell morphology and increased motility were seen.

Progress towards orthogonal light-induced activation

The ultimate goal of this work is to create tools to better understand immune activation mechanisms. Ongoing research in the Esser-Kahn group aims to combine these and other light-controllable agonists described previously to uncover the spatial and temporal aspects of signaling, specifically in synergies. The work described herein is the first step toward generating agonists that can be used orthogonally to generate synergies in a controlled manner. The synergy between TLR4 and 7, 8 activation pathways is evident in immune cells treated with both TLR4 and 7,8 agonists (**Figure 3.8**), and has been confirmed in other studies.[11,16] The next steps are to synthesize caged agonists with two-photon photo-labile protecting groups, such as courmarin-based cages,[17] and use two-photon deprotection to selectively uncage these molecules, controlling time and/or space, to determine the source of the synergistic interactions (**Figure 3.9**).

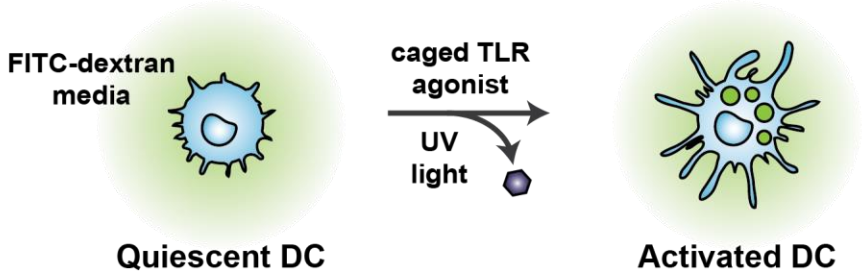

Figure 3.6. Scheme of light-controlled endocytosis in BMDCs. Cells were treated with caged agonist **6** in media supplemented with fluorescent (FITC) dextran, and sandwiched between coverslips. Cells were exposed to UV light (365 nm) and immediately imaged by confocal microscopy.

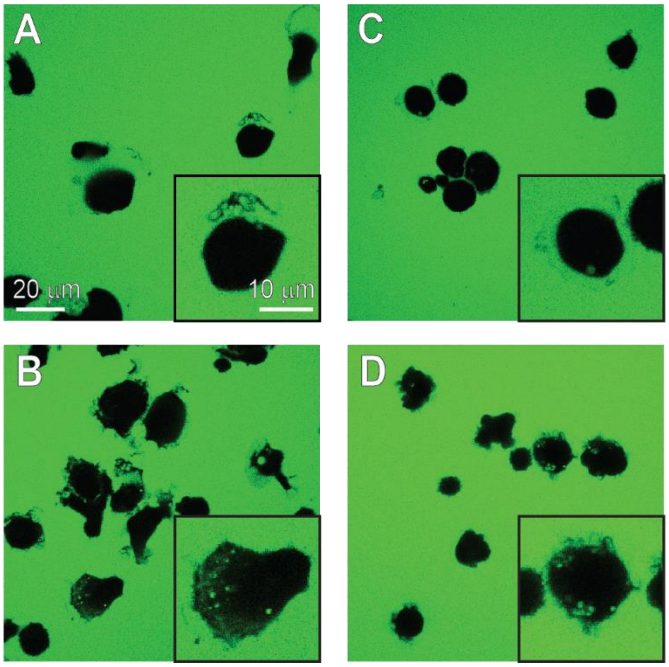

Figure 3.7. Light-controlled endocytosis in BMDCs. Cells were treated with media supplemented with fluorescent (FITC) dextran without agonist (**A**), with TLR7 and 8 agonist **4** (**B**), or TLR7 and 8 caged agonist **6** without (**C**) and with UV light exposure (**D**). The scale bars are equal to 20 μm (insets 10 μm). Cells treated with **6** without UV light exposure showed a small number of endosomes. Activation of cells was observed as early as 10 min after treated with **4** or **6** with UV light exposure, showing a change in cell morphology and a large number of endosomes.

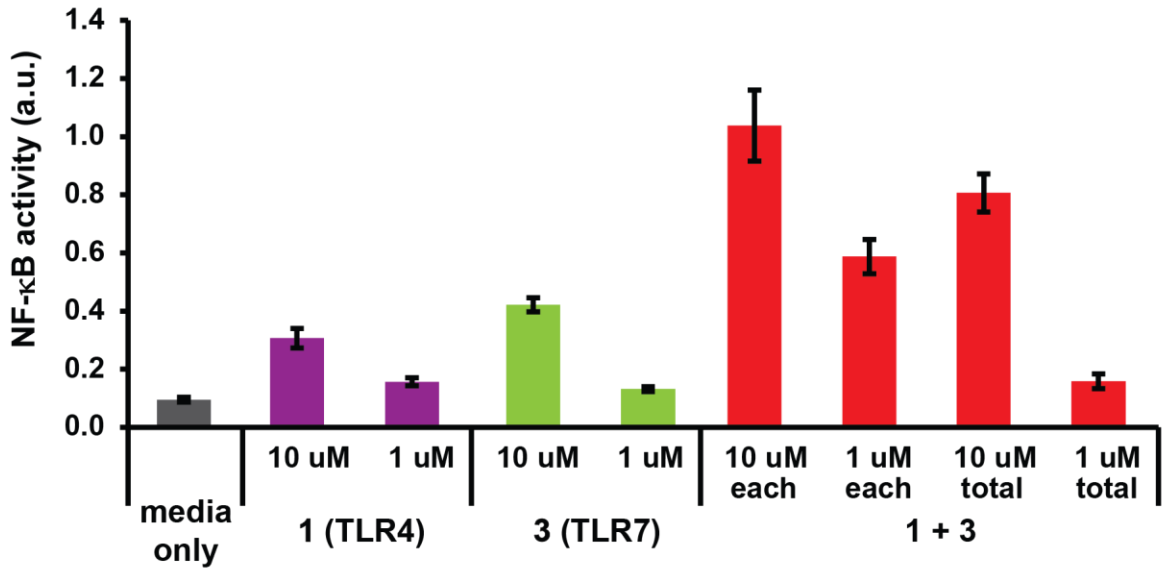

Figure 3.8. Activation of NF-κB pathway in RAW-Blue macrophages after treatment with TLR4 and 7 agonists. Cells were treated with media only (black), **1** (1 or 10 µM; purple), **3** (1 or 10 µM; green), or a combination of **1** and **4**. NF-κB activation was determined using the SEAP colorimetric assay (OD measured at 620 nm). Each experiment was performed in replicates of three. Activation of NF-κB was greatest in cells treated with both agonists. Responses that were more than additive of those of the individual agonists imply immune synergies or inflammation networks.

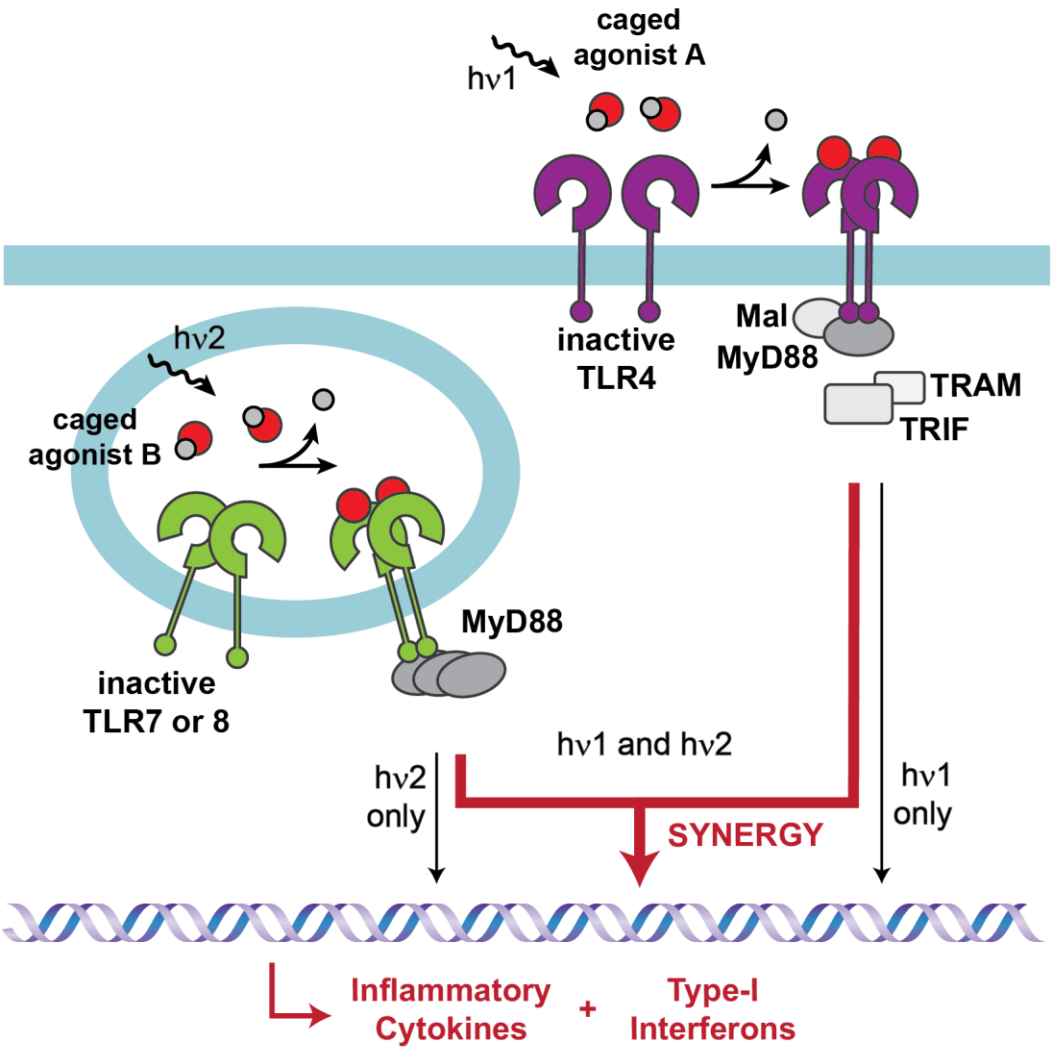

Figure 3.9. Scheme of activation pathways using orthogonal caged TLR agonists. Immune synergies may be characterized by activating cells controlling spatial and temporal aspects through selective deprotection of caged agonists.

Summary of spatially-controlled immune activation using a caged TLR7 and 8 agonists

In this work, I described the synthesis and an example of photo-controlled activation of TLR7 and 8. Protection of the critical nitrogen's of imiquimod and resiquimod with photo-labile groups reduced NF-κB activity to background levels. Upon exposure to UV light, the parent agonists were regenerated, which then activated NF-κB signaling pathways via TLR7 or 8. We showed activation of innate immune cells, RAW macrophages and BMDCs, can be mediated by UV light exposure of the caged agonist.

References

(1) Diebold, S. S. *Science* **2004**, *303* (5663), 1529–1531.
(2) Hemmi, H.; Kaisho, T.; Takeuchi, O.; Sato, S.; Sanjo, H.; Hoshino, K.; Horiuchi, T.; Tomizawa, H.; Takeda, K.; Akira, S. *Nat. Immunol.* **2002**, *3* (2), 196–200.
(3) Elavazhagan, S.; Fatehchand, K.; Santhanam, V.; Fang, H.; Ren, L.; Gautam, S.; Reader, B.; Mo, X.; Cheney, C.; Briercheck, E.; Vasilakos, J. P.; Dietsch, G. N.; Hershberg, R. M.; Caligiuri, M.; Byrd, J. C.; Butchar, J. P.; Tridandapani, S. *J. Immunol.* **2015**, *194* (6), 2786–2795.
(4) Latz, E.; Verma, A.; Visintin, A.; Gong, M.; Sirois, C.; Klein, D.; Monks, B.; McKnight, C. J.; Lamphier, M.; Duprex, P.; Espevik, T.; Golenbock, D. *Nature* **2007**, *8*, 772–779.
(5) Wei, T.; Gong, J.; Jamitzky, F.; Heckl, W.; Stark, R.; Rossle, S. *Protein Sci* **2009**, *18* (8), 1684–1691.
(6) Tanji, H.; Ohto, U.; Shibata, T.; Miyake, K.; Shimizu, T. *Science* **2013**, *339* (6126), 1426–1429.
(7) Chan, M.; Hayashi, T.; Mathewson, R. D.; Yao, S.; Gray, C.; Tawatao, R. I.; Kalenian, K.; Zhang, Y.; Hayashi, Y.; Lao, F. S.; Cottam, H. B.; Carson, D. A. *Bioconjug. Chem.* **2011**, *22* (3), 445–454.
(8) Chan, M.; Hayashi, T.; Kuy, C. S.; Gray, C. S.; Wu, C. C. N.; Corr, M.; Wrasidlo, W.; Cottam, H. B.; Carson, D. A. *Bioconjug. Chem.* **2009**, *20* (6), 1194–1200.
(9) Kokatla, H. P.; Sil, D.; Malladi, S. S.; Balakrishna, R.; Hermanson, A. R.; Fox, L. M.; Wang, X.; Dixit, A.; David, S. A. *J. Med. Chem.* **2013**, *56* (17), 6871–6885.
(10) Shukla, N. M.; Salunke, D. B.; Balakrishna, R.; Mutz, C. A.; Malladi, S. S.; David, S. A. *PLoS ONE* **2012**, *7* (8), e43612.
(11) Garcia-Cordero, J. L.; Nembrini, C.; Stano, A.; Hubbell, J. A.; Maerkl, S. J. *Integr. Biol. Quant. Biosci. Nano Macro* **2013**, *5* (4), 650–658.
(12) Gibbard, R. J.; Morley, P. J.; Gay, N. J. *J Biol Chem* **2006**, *281*, 27503–27511.
(13) Ryu, K. A.; Stutts, L.; Tom, J. K.; Mancini, R. J.; Esser-Kahn, A. P. *J. Am. Chem. Soc.* **2014**, *136* (31), 10823–10825.
(14) Chan, M.; Hayashi, T.; Mathewson, R. D.; Nour, A.; Hayashi, Y.; Yao, S.; Tawatao, R. I.; Crain, B.; Tsigelny, I. F.; Kouznetsova, V. L.; Messer, K.; Pu, M.; Corr, M.; Carson, D. A.; Cottam, H. B. *J. Med. Chem.* **2013**, *56* (11), 4206–4223.
(15) West, M. A.; Wallin, R. P. A.; Matthews, S. P.; Svensson, H. G.; Zaru, R.; Ljunggren, H.-G.; Prescott, A. R.; Watts, C. *Science* **2004**, *305* (5687), 1153–1157.
(16) Napolitani, G.; Rinaldi, A.; Bertoni, F.; Sallusto, F.; Lanzavecchia, A. *Nat. Immunol.* **2005**, *6* (8), 769–776.
(17) Zhao, Y.; Zheng, Q.; Dakin, K.; Xu, K.; Martinez, M. L.; Li, W.-H. *J. Am. Chem. Soc.* **2004**, *126* (14), 4653–4663.

CHAPTER 4: Cell labeling and controlled activation with TLR1, 2, and 6 agonists

Overview of TLR1, 2, and 6 signaling

Receptor structure and agonists

Toll-like receptor 2 is an outer-membrane bound PRR that detects cell wall components of Gram-positive bacteria. Dissimilar to other known TLRs, TLR2, upon ligand binding, pairs with either TLR1 or TLR6 to form a functional heterodimer. Activators of TLR1/2 are primarily lipid-based molecules, while TLR2/6 interact with lipid and some non-lipid agonists through polar binding regions of TLR6.[1,2] The hydrophobic binding pockets of TLR1 and 2 interact with lipid chains of bacterial lipidated peptides and proteins (**Figure 4.1**). A lipid moiety of an agonist associates with both of the TLRs of the 1/2 heterodimer pair, but only TLR2 of the 2/6 pair.

The exogenous ligands of TLR1, 2 and 6 are palmitylated lipopeptides and proteins (**Figure 4.2**). The number of lipids decorated on peptide or protein agonists vary. In general, agonists composed of tri-palmitylated lipopeptide sequences bind and potently activate TLR1 complexes. TLR2 binds more promiscuously to mono-, di-, and tri-palmitylated sequences, including lipoteichoic acids (LTA) and lipoarabinomannans.[3] Lipoteichoic acids are also recognized by TLR6 and are a mixture of acylated glycopeptides composed of N-acetylglucosamine (GlcNAc) and alanine residues along a polymeric phosphate backbone.[4]

In addition to native immunostimulants, a variety of synthetic mimics have also been developed to activate TLR1, 2, and 6 (**Figure 4.2**). Commonly used agonists are synthetic palmityl-substituted cysteine-serine-lysine (PAM_2CSK_4 and PAM_2CSK_4) derivatives of the native agonists.[5] Variations to the lipid chains of TLR1 agonists have been explored.[6,7] Potency of agonists with a triacylated *N*-terminal cysteine was found to be greatest with acyl chains 16 carbons

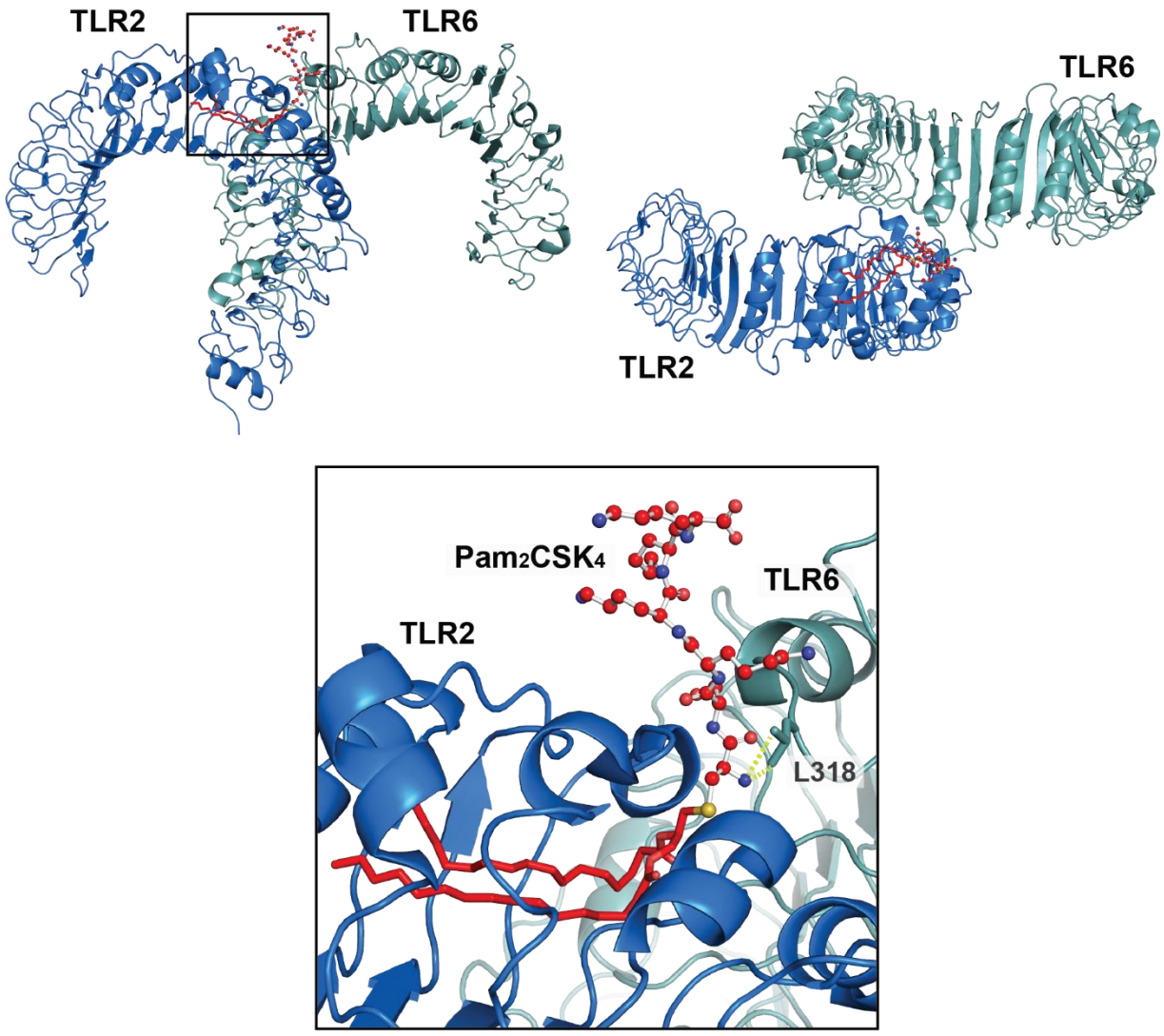

Figure 4.1. Crystal structure of TLR2/6 with Pam_2CSK_4. The lipid chains of lipopeptide agonists interact with TLR2, while the peptide residues bind TLR6. The *N*-terminal cysteine reside of Pam_2CSK_4 hydrogen bonds with L318 of TLR6 and is critical for activation.

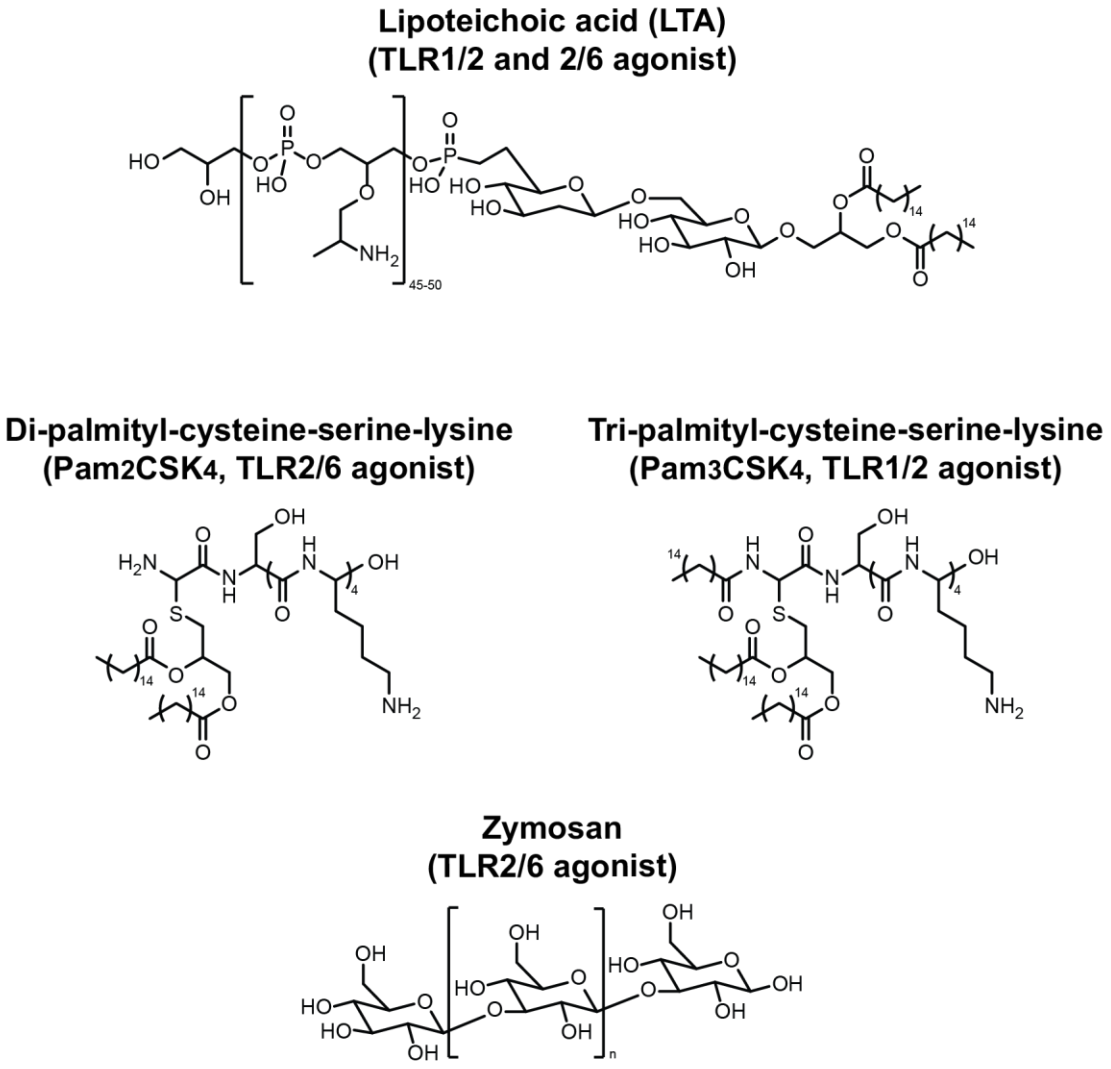

Figure 4.2. Common TLR1, 2, and 6 agonists. Palmityl-substituted peptide agonists and others have specificity of TLR1/2 or 2/6 binding and activation. In TLR1/2 activation, two palmityl chains of Pam_3CSK_4 interact with TLR2, leaving the other to interact with TLR1. Conversely, the two palmityl chains of Pam_2CSK_4 only interact with TLR2 in the TLR2/6 heterodimer.

long. Diacyl chains of 6-18 carbon length bind TLR2, and C-16 lipids, again, are the most potent stimulators.[8]

Other, non-lipid agonists have been shown to activate through TLR1, 2, and 6. Zymosan (a mixture of β-1,3 glucans), and other polysaccharides activate through polar interactions with the receptors.[9–11]

TLR1, 2, and 6 signaling

TLR1, 2, and 6 activation pathway occurs through MyD88 (**Figure 4.3**).[12] Like TLR4, TLR1/2 and TLR2/6 complexes require the Mal adapter for signal transduction.[13] Upon ligand binding and receptor dimerization, Mal and MyD88 associate with the TIR domains. These signaling molecules stimulate downstream pathways involving IRAKs, TRAFs, and MKKs. The end results of TLR1, 2, 6 activation is the activation of the pro-inflammatory-related transcription factors NF-kB, AP1, and CREB.

Probing TLR2 activation mechanisms

An interesting facet of TLR signaling is that some non-immune cells express TLRs, including TLR1, 2, and 6, and corresponding activation and transcriptional proteins. The proposed explanation for this is that tissues contribute to inflammatory signaling to help activate and recruit immune cells.[14] TLR activation in non-immune cells has been observed in the skin, and respiratory and intestinal tracts. Non-immune cells known to express TLRs include epithelial, endothelial, smooth muscle, and fibroblast cells. The mechanisms of non-immune cells cooperate with the immune system to produce robust inflammatory signals is unknown. As such, studying

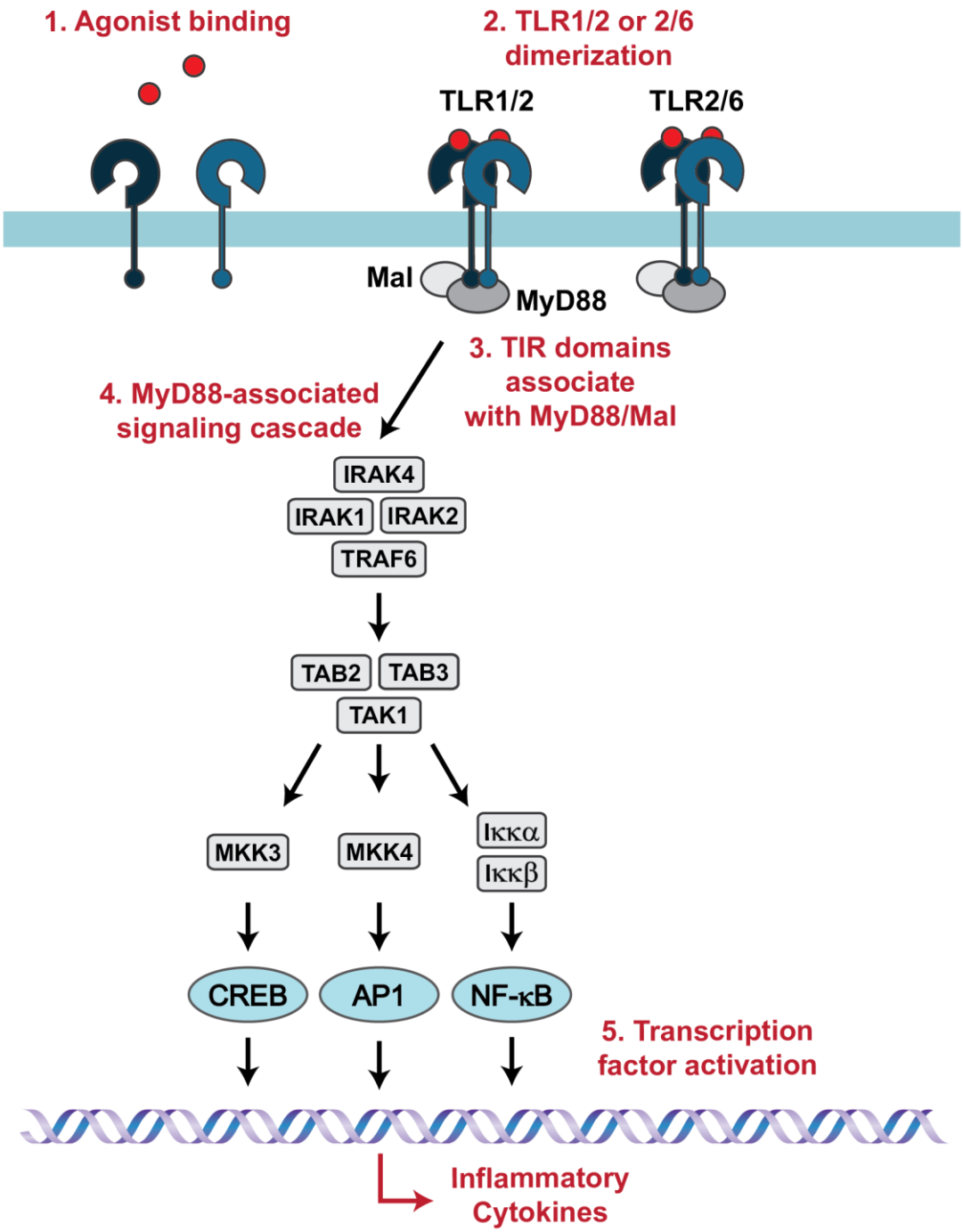

Figure 4.3. TLR1, 2, and 6 signaling pathways. Activation of TLR1/2 and 2/6 results in signaling of the MyD88 pathway and upregulations of inflammatory cytokines.

inflammation using traditional immunostimulants is complicated by paracrine and autocrine signaling that obscures the origin and propagated response.

Here, a novel immunostimulant was designed using the same light-controlled approach described in previous sections. The TLR2/6 agonist, PAM_2CSK_4, was modified with a photo-labile protecting group, NPPOC, at a position critical for receptor activation to employ the agonist in a light-controlled manner (**Figure 4.4**). Structure-activity studies indicated substitution at the *N*-terminus is not tolerated.[15] Additionally, analysis of the TLR2/6 crystal structure showed that the interaction between the L318 residue of TLR6 and the *N*-terminus of Pam_2CSK_4 is important for binding and dimerization (**Figure 4.1**).[16] We hypothesized that protection of the *N*-terminal amine to a photo-labile protecting group would disrupt TLR2/6 dimerization, and therefore, activation. The palmityl chains Pam_2CSK_4 were purposely left unmodified to allow the molecules to still interact with the lipid binding pockets. This docking afforded specific cell labeling with the caged agonist without activation. The four lysine residues of Pam_2CSK_4 do not interact with either receptor, and therefore, was installed a 5/6-carboxyfluorescein (FAM) fluorophore to the terminal residue to track the probe in cell experiments.[17]

The aim of developing and applying this caged agonist deviates from those described previously relating to spatial and temporal activation. This probe was used to label either immune or mural cells, and control the origins of inflammation in a heterogeneous culture of immune and non-immune cells (**Figure 4.5**). With the caged TLR agonist capable of both cell labelling and controlled activation, we hoped to better understand the roles of non-immune cells in immune signal propagation.

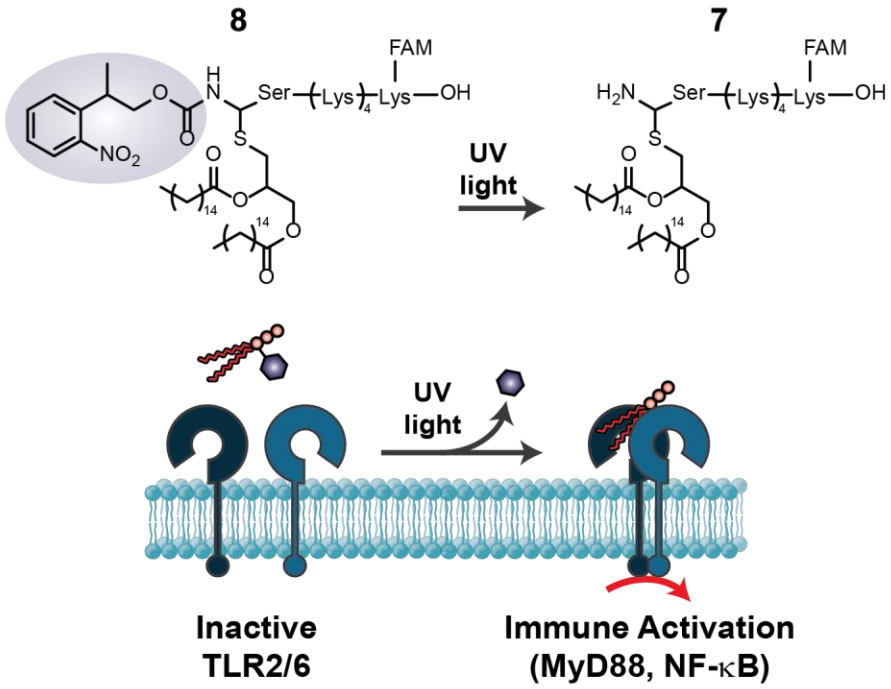

Figure 4.4. Photo-controlled deprotection of caged TLR2/6 agonist. NPPOC-caged Pam_2CSK_5(FAM) **8** is converted to **7** using UV light (365 nm) to activate immune cells via TLR2/6.

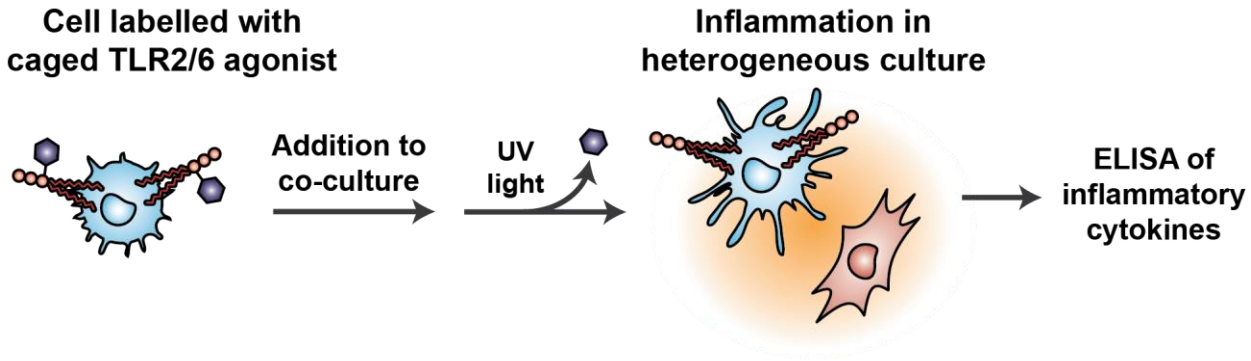

Figure 4.5. Scheme of light-controlled activation in co-cultures of BMDCs and fibroblasts. One cell type was labelled with caged TLR2/6 agonist **8**, combined with the second cell type, and the co-culture was deprotected with UV light (365 nm). Inflammation was assessed by TNF secretion, as determined by ELISA of cell supernatant.

Design and characterization of a caged TLR2/6 agonist

Synthesis of the caged TLR2/6 agonist

The synthesis and characterization of caged TLR2/6 agonist **8** was performed by Dr. Rock Mancini. Briefly, caged di-palmitylated cysteine was synthesized in 8% yield from cystine di-*t*-butyl ester over 5 steps. The synthesis began with addition of NPPOC-chloroformate to di-*tert*-butyl cystine. This reaction was followed by reduction of the disulfide and addition of excess 1-bromo-2,3-propanediol to afford in 42% yield (2 steps). Subsequent palmitylation and removal of the *tert*-butyl protecting group provided the terminal amino acid, NPPOC-di-palmityl-cysteine in 21% yield (2 steps). Wang resin pre-loaded with *N*-ε-(FAM)-lysine was used to install the serine-tetra-lysine (SK_4) sequence before capping with the caged-palmityl-cysteine over 24 h. Global deprotection and resin cleavage provided the fluorescent, photo-caged sequence NPPOC-$C(Pam)_2SK_5$(FAM)-OH **8**. Protection of the *N*-terminus of Pam_2CSK_4 was confirmed *via* high-resolution mass spectrometry, and ^{1}H and ^{13}C NMR spectroscopy.[18]

Deprotection of **8** to form the parent compound **7** was verified by UV/Vis and HPLC analysis. Formation of **7** was reformed (over 90% conversion) after 15 min irradiation with UV light (4 W, 365 nm).[18]

Cell labelling and activation using light

Preliminary assessment of immune activation

Activation of the NF-kB pathway in immune cells using the light-controlled agonist was tested in RAW-Blue macrophages (**Figure 2.8**). We predicted minimal activity in cells treated with caged agonist, as the dimerization would be obscured by protection of the agonists *N*-terminus. Removal of the NPPOC protecting group would afford active agonist and elicit an

immune response. Cells were treated with **8** (1 and 10 ng/mL) with and without UV light exposure 4 W, 365 nm) for 10 min. Treatment with **8** and exposure to UV light resulted in high levels of NF-kB activity, while **8** without UV exposure showed basal levels of activation (**Figure 4.6**).

Cell labelling and light-controlled activation with caged TLR2/6 agonist

To study the origins of inflammation in heterogeneous cell cultures, immune and non-immune cells were first labelled with the caged TLR2/6 agonist. In these experiments, the immune cells were bone marrow-derived dendritic cells (BMDCs) and the non-immune cells were fibroblasts. Both cell types express TLR2 and 6. Cell labelling was observed by confocal microscopy. The fluorescent tag of the caged agonist was seen in cells treated with **8**, primarily distributed on cell surfaces (**Figure 4.7**).

The contribution of different signaling molecules in fibroblast-immune cell signaling, such as TNF or prostanoids remain ill-defined.[19,20] Here, immune activation was assessed by the measurement of a common pro-inflammatory cytokine, tumor necrosis factor α (TNF). TNF secreted by co-cultures of BMDCs and fibroblasts, where one cell type was labelled with caged agonist, was measured (**Figure 4.8**). This approach allowed quantification of TNF production due to direct activation of BMDCs with immunostimulant relative to activation via TLR-activated fibroblast intercellular signaling. We expected that cooperativity would be observed in heterogeneous cell cultures and elicit a greater immune response compared to homogeneous cell cultures.

Differences in TNF secretion were observed depending on the initiating cell type. BMDCs that were labelled and stimulated alone produced TNF (48 pg/mL) while fibroblasts that were labelled and stimulated alone did not produce a detectable amount of cytokine. BMDCs that were

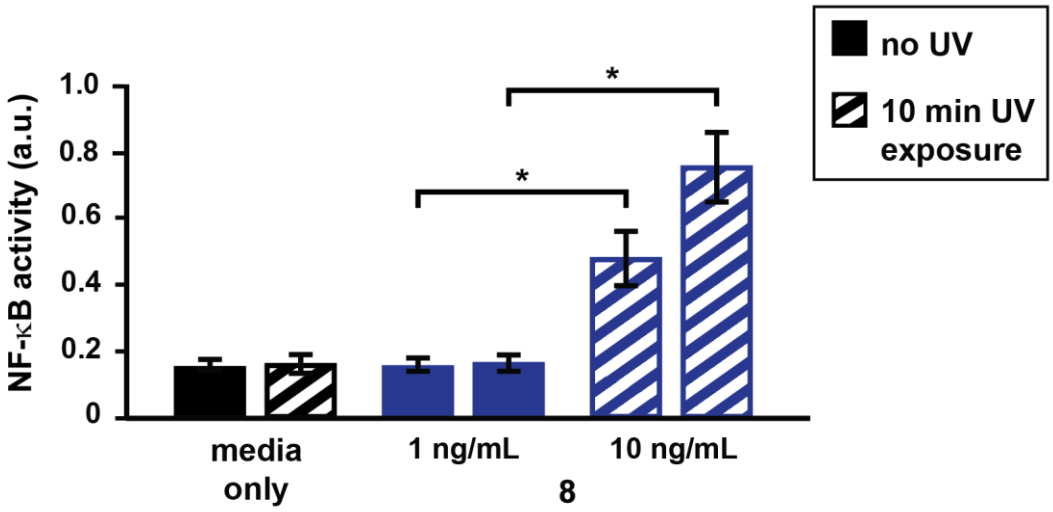

Figure 4.6. Light-controlled NF-κB activation in reporter cells, RAW-Blue macrophages. Caged agonist **8** does not activate TLR2/6 until photo-controlled deprotection with UV light. Cells were treated with media only (black), **8** (1 or 10 ng/mL; blue), without (solid) or with (outlined) UV light exposure (15W, 365 nm light). NF-κB activation was determined using the SEAP colorimetric assay (OD measured at 620 nm). Each experiment was performed in replicates of five (*$p < 0.01$).

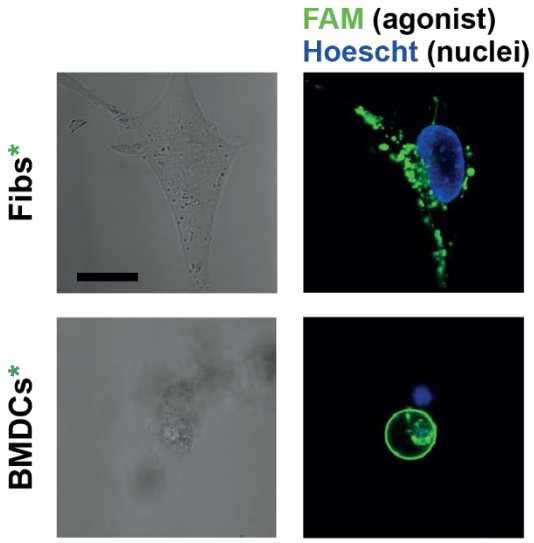

Figure 4.7. Cell labelling using the caged TLR2/6 agonist **8**. Fibroblasts and BMDCs were labelled with Pam_2CSK_5(FAM) and stained with Hoescht Blue. Cell labelling was observed by confocal microscopy (bright field, left; fluorescent channels, right). Labelled cells are denoted with a *. The scale bar is equal to 10 µm.

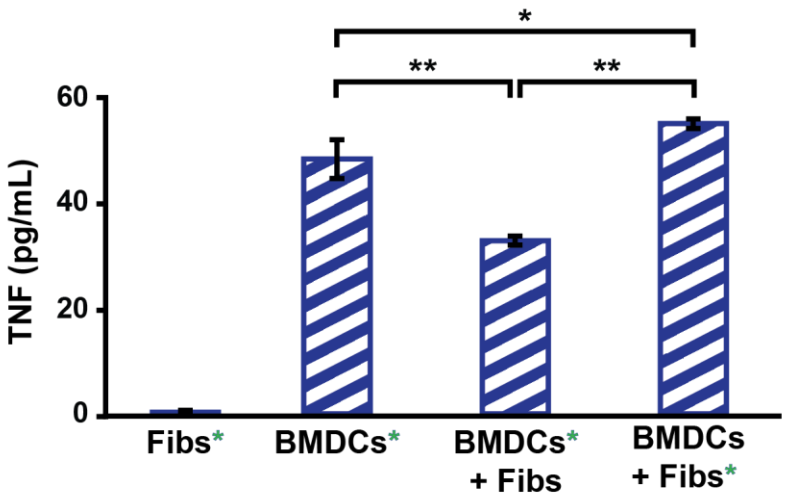

Figure 4.8. TNF secretion by labelled and activated BMDC and fibroblast homo- and heterogeneous cultures. Labelled cells are denoted with a *. Deprotected caged agonist **8** causes secretion of TNF in cultures of labelled BMDCs, but not labelled fibroblasts. Differences in activation are observed in mixed cultures. Each experiment was performed in replicates of six (*$p < 0.025$ and **$p < 0.001$).

labelled and stimulated in the presence of fibroblasts, showed a significantly lower amount (30 pg/mL) of TNF than the BMDC alone samples. Interestingly, fibroblasts that were labelled and stimulated in the presence of BMDCs yielded the most amount of TNF (56 pg/mL). This result indicates that inflammation is sensitive to the originating TLR signal. This finding could imply that targeting mural cells, such as fibroblasts, rather than or in addition to immune cells might be a better approach in designing adjuvants and/or treating inflammation.

Summary

In this work, we showed the synthesis and application of a light-controlled immunostimulant of TLR2/6. We studied the origin of inflammation in heterogeneous cell populations, where one of two of the cell types were labelled and activated using a light-controlled TLR2/6 agonist, Pam_2CSK_4. This approach mirrors inflammation in tissues during infection, which is proposed to occur through both immune and mural cells. Measurements of the inflammation-associated cytokine, TNF, secreted from co-cultures of BMDCs and fibroblasts demonstrated that activation of immune cells can occur indirectly though TLR-stimulated mural cells, in addition to the conventional direct method of TLR-stimulation of the immune cells.

References

(1) Jin, M. S.; Kim, S. E.; Heo, J. Y.; Lee, M. E.; Kim, H. M.; Paik, S.-G.; Lee, H.; Lee, J.-O. *Cell* **2007**, *130* (6), 1071–1082.

(2) Kang, J. Y.; Nan, X.; Jin, M. S.; Youn, S.-J.; Ryu, Y. H.; Mah, S.; Han, S. H.; Lee, H.; Paik, S.-G.; Lee, J.-O. *Immunity* **2009**, *31* (6), 873–884.

(3) Zaehringer, U.; Lindner, B.; Inamura, S.; Heine, H.; Alexander, C. *Immunobiology* **2008**, *213* (3-4), 205–224.

(4) Ginsburg, I. *Lancet Infect. Dis.* **2002**, *2* (3), 171–179.

(5) Wiesmuller, K.; Bessler, W.; Jung, G. *Hoppe. Seylers Z. Physiol. Chem.* **1983**, *364* (5), 593–606.

(6) Berg, M.; Offermanns, S.; Seifert, R.; Schultz, G. *Am. J. Physiol.* **1994**, *266* (6), C1684–C1691.

(7) Agnihotri, G.; Crall, B. M.; Lewis, T. C.; Day, T. P.; Balakrishna, R.; Warshakoon, H. J.; Malladi, S. S.; David, S. A. *J. Med. Chem.* **2011**, *54* (23), 8148–8160.

(8) Salunke, D. B.; Shukla, N. M.; Yoo, E.; Crall, B. M.; Balakrishna, R.; Malladi, S. S.; David, S. A. *J. Med. Chem.* **2012**, *55* (7), 3353–3363.

(9) Sahoo, B. R.; Basu, M.; Swain, B.; Dikhit, M. R.; Jayasankar, P.; Samanta, M. *BioMed Res. Int.* **2013**, *2013*.

(10) Tsai, C.-C.; Lin, C.-R.; Tsai, H.-Y.; Chen, C.-J.; Li, W.-T.; Yu, H.-M.; Ke, Y.-Y.; Hsieh, W.-Y.; Chang, C.-Y.; Wu, C.-Y.; Chen, S.-T.; Wong, C.-H. *J. Biol. Chem.* **2013**, *288* (24), 17689–17697.

(11) Gantner, B. N.; Simmons, R. M.; Canavera, S. J.; Akira, S.; Underhill, D. M. *J. Exp. Med.* **2003**, *197* (9), 1107–1117.

(12) O'Neill, L. A. J.; Golenbock, D.; Bowie, A. G. *Nat. Rev. Immunol.* **2013**, *13* (6), 453–460.

(13) O'Neill, L. A. J.; Dunne, A.; Edjeback, M.; Gray, P.; Jefferies, C.; Wietek, C. *J. Endotoxin Res.* **2003**, *9* (1), 55–59.

(14) Parker, L. C.; Prince, L. R.; Sabroe, I. *Clin. Exp. Immunol.* **2007**, *147* (2), 199–207.

(15) Wu, W.; Li, R.; Malladi, S. S.; Warshakoon, H. J.; Kimbrell, M. R.; Amolins, M. W.; Ukani, R.; Datta, A.; David, S. A. *J. Med. Chem.* **2010**, *53* (8), 3198–3213.

(16) Kang, J. Y.; Nan, X.; Jin, M. S.; Youn, S.-J.; Ryu, Y. H.; Mah, S.; Han, S. H.; Lee, H.; Paik, S.-G.; Lee, J.-O. *Immunity* **2009**, *31* (6), 873–884.

(17) Prass, W.; Ringsdorf, H.; Bessler, W.; Wiesmüller, K.-H.; Jung, G. *Biochim. Biophys. Acta BBA - Biomembr.* **1987**, *900* (1), 116–128.

(18) Mancini, R. J.; Stutts, L.; Moore, T.; Esser-Kahn, A. P. *Angew. Chem. Int. Ed.* **2015**, *54* (20), 5962–5965.

(19) Berthier, R.; Rizzitelli, A.; Martinon-Ego, C.; Laharie, A. M.; Collin, V.; Chesne, S.; Marche, P. N. *Immunology* **2003**, *108* (3), 391–400.

(20) Landi, A.; Babiuk, L. A.; Littel-van den Hurk, S. van D. *Immunobiology* **2011**, *216* (6), 649–662.

CHAPTER 5: Final remarks

Research in the field of immunology has greatly expanded in recent decades. The major contributions have been in the discovery of receptors, including Toll-like receptors (TLRs), and signaling proteins involved in activation cascades. Additionally, a number of immunostimulants have been identified and synthetically elaborated upon to better understand pathogen binding and the effects on immune activation. An overarching theme in studying both ligands and pathways is that of immune synergies. It is hypothesized that, like many other biochemical pathways, feedback loops and synergistic networks are the source of the complex activation outcomes resulting from multiple agonists and pathways acting on a cell.

Research in the Esser-Kahn group has focused on generating chemical tools for studying the immune system. Herein, I have described the development of small molecules for elucidating spatial and temporal details of immune activation. Spatial and temporal control of activation is achieved by installation of photo-labile protecting groups to TLR agonists. Inspired by and elaborating upon structural-activity studies, crystallographic data, and *in silico* docking experiments of various TLR immunostimulants, we first determined the most crucial moieties of these molecules for receptor interaction. Next, we targeted these functional groups for protection with photo-labile protecting groups. We found that caging the indole nitrogen of pyrimido indole (TLR4 agonist), the primary amine of imidazoquinolines (TLR7 and 8 agonists), and the *N*-terminus of PamCSK (TLR2/6 agonist) rendered them non-stimulatory in immune cells. Deprotection of the cage via UV light exposure, reestablished activation of the major immune signaling pathway, NF-κB, comparable to levels in cells treated with the active parent agonists.

The first example of a photo-controlled agonist described herein was designed around a small molecule TLR4 agonist, pyrimido[5,4-*b*]indole. Agonists for TLR4 were targeted because this receptor has been identified as critical for effective immune responses. Additionally, the downstream signaling pathways of TLR4 are unique and complex, and the spatial and temporal components of these pathways are not well understood. Protection of the critical indole nitrogen with a photo-labile group, 6-nitroveratryloxycarbonyl (NVOC), reduced NF-κB activity to background levels in two TLR4-bearing NF-κB reporter cell lines, RAW-Blue macrophages and p65-DsRed fibroblasts. Light-controlled spatial activation was demonstrated by selective exposure of a subpopulation of cells using a pinhole mask. This resulted in NF-κB stimulation of select patches of cells.

Next, I showed the development and application of photo-controlled TLR7 and 8 agonists. These receptors were targeted because they are proposed to act in synergy with TLR4, presumably via simultaneous activation of their disparate signaling pathways. We hypothesized that order and timing of these pathway relative to one another play a very important role in eliciting strong immune responses. Protection of the critical nitrogen's of imiquimod and resiquimod with photo-labile groups, 2-(2-nitrophenyl)propyloxycarbonyl (NPPOC), reduced immune activity to background levels. We showed that activation of innate immune cells, RAW macrophages, as well as primary dendritic cells (BMDCs), is mediated by UV light exposure of the caged agonist.

A light-controlled immunostimulant of TLR2/6 is also described. With a lipid-based caged Pam_2CSK_4 variant, we labelled cells and used light to control the origin of inflammation in heterogeneous cell populations. Co-cultures of BMDCs (innate immune cells) and fibroblasts (non-immune cells prevalent in many tissues) demonstrated that activation of immune cells can occur indirectly though TLR-stimulated mural cells, in addition to the conventional direct method

of TLR-stimulation of the immune cells. Through this approach, we sought to replicate *in vitro* the inflammation in tissues on the onset of infection, where TLR-bearing non-immune cells are thought to be a major contributor in facilitating the initial response against a pathogen.

This preliminary work designing and testing NVOC- and NPPOC-protected agonists has successfully established a method for spatial and temporal control of TLR-based immune activation. Progress towards elaborating upon caged agonists is continued by other members of the Esser-Kahn group. The future work involves the generation of agonists with orthogonally-photo-labile cages. The aim is to utilize the high degree of control and precision of two-photon microscopy to deprotect agonists *in vitro*. Selective activation of receptors can be achieved within populations of cells, or even in a single cell. These tools and methods have the potential to be widely applied by immunologists to elucidate the many unknowns of individual pathways, synergies and global immune system activation.

APPENDIX A

Materials

Chemical reagents, as well as Fetal Bovine Serum (FBS) and Heat-Inactivated FBS (HI-FBS), were purchased from Sigma-Aldrich, unless otherwise specified. Cell culture reagents were purchased from Life Technologies. The RAW-Blue 264.7 Macrophages, Zeocin, and QUATI-Blue reagent were purchased from Invivogen. The p65-DsRed fibroblasts were donated by Prof. Markus Covert. Agonists were stored in DMSO, maintained at -80 °C with a minimal number of freeze/thaw events.

Synthesis

Synthesis of TLR4 agonist **1**

The TLR4 agonist, pyrimido[5,4-*b*]indole **1** was synthesized and purified as described previously.[1]

Synthesis of caged TLR4 agonist **2**

In a flame-dried flask, **1** (200 mg, 0.46 mmol) was combined with NaH (60% dispersed in mineral oil, 100 mg, 2.5 mmol) in 2 mL dry THF and stirred at room temperature for 30 min. 4,5-dimethoxyl-2-nitrobenzyl chloroformate (251 mg, 0.91 mmol) was dissolved in 10 mL dry THF and added to the reaction flask. The mixture was heated to reflux for 3 h. The reaction was quenched with water and the crude product was extracted with methylene chloride. The product was purified by column chromatography with methylene chloride/20% acetonitrile to obtain 164 mg **2** (53.1% yield).

Synthesis of TLR7 agonist **5**

Imiquimod (0.03 g, 0.2 mmol, LKT Technologies) was stirred with 3 mL of anhydrous 1,4

dioxane and the solution was cooled to 10 °C. 2-(2-nitrophenyl)propyloxycarbonyl chloride (NPPOC-Cl, 0.0608 g, 0.4 mmol,) was diluted with 1 mL of anhydrous 1, 4 dioxane (2 mL). The NPPOC-Cl solution was added dropwise to the agonist solution. The resulting solution was heated to 50 °C for 6 hr. Reaction was monitored via TLC. The resulting products were purified by column chromatography (10% MeOH/DCM) and concentrated under vacuum. Resulted in 0.020g (38 % yield) as yellow oil.

Synthesis of TLR7 and 8 agonist **6**

Followed same reaction procedures as NPPOC-imiquimod with adjusted amounts of reagents. Resiquimod (30 mg, 0.1 mmol) was stirred in anhydrous 1,4 dioxane at 10 °C. NPPOC-Cl (47 mg, 0.2 mmol) was diluted in anhydrous 1, 4 dioxane and added dropwise to the agonist solution. The reaction mixture was heated to 50 °C for 6 hr. The solution was concentrated under vacuum and purified by silica gel column chromatography to obtain **6** (16 % yield).

Characterization of deprotection of caged TLR4 agonist

The uncaging efficiency of **2** was examined by UV absorption and HPLC of the TLR4 agonist **1** and caged agonist **2** before and after UV exposure. Solutions for both methods were prepared in 10:1 (v:v) DMSO:H_2O. Samples were exposed to direct light (15 W, 365 nm), with the lamp positioned 1 cm from the sample.

To characterize the major species in solution, we performed HPLC analysis of **1**, **2** before and after UV exposure. Samples were eluted using an acetonitrile and water gradient varying from 10:90 to 90:10 (ACN:H_2O) over 20 min at a rate of 5 mL/min. The detector was set at 250 nm for the signal acquisition, consistent with the UV-Vis characterization that showed local maxima at 250 nm for both **1** and **2** with and without UV light exposure. **1**, **2** had elusion times of 13.5 and

17.1 min, respectively. Confirmation of these LC peaks were performed using mass spectrometry. The compound with an elusion time of 13.5 min corresponded to ($M_{TLR4\ agonist}$+1) = 433, and the compound with an elusion time of 17.1 min corresponded to ($M_{caged\ agonist}$+1) = 640. The amounts of **1** and **2** was determined by integrating the area of LC trace corresponding to each species. Percent conversion was calculated using these integrated values. The 30 min deprotection experiment was performed in replicates of three. HPLC and MS characterization did not detect the significant formation of side products. Additionally, to confirm consistent sample preparation and instrument injection, an internal standard, methyl indole-5-carboxylate, was added to sample before HPLC analysis.

Cell culture

RAW-Blue 264.7 macrophages

RAW-Blue cells were cultured in complete culture media, consisting of Dulbecco's Modified Eagle Medium (DMEM, high glucose) supplemented with 10% FBS, 10,000 U/mL penicillin, 10 mg/mL streptomycin, 25 µg/mL amphotericin B, and 200 µg/mL Zeocin. Cells were maintained at 37 °C and 5% CO_2 and used within passage 4-8 for all experiments. Complete test media for these cells was composed of DMEM (high glucose) supplemented with 10% HI-FBS.

3T3 fibroblasts

Fibroblasts were cultured in complete culture media, consisting of DMEM (high glucose) supplemented with 20% FBS, 10,000 U/mL penicillin, 10 mg/mL streptomycin, and 25 µg/mL amphotericin B. Cells were maintained at 37 °C and 5% CO_2. Complete test media for these cells was composed of DMEM with 4.5 g/L glucose and 1% HI-FBS.

Bone marrow-derived dendritic cells

BMDCs were harvested from 6-week-old C57Bl/6 mice (Jackson Laboratory). Femur bones were removed from mice and the bone marrow was extracted into phosphate-buffered saline (PBS) buffer. The cell suspension was made into a homogeneous solution using a pipette and subsequently filtered through a 70 μm cell strainer. The cell solution was centrifuged at 300 RCF for 10 min at RT. The supernatant was removed, and ACK Lysing Buffer (3 mL, Lonza) was added to the cell pellet and incubated for 2 min at RT. PBS buffer (13 mL) was then added to the cell suspension, and the cell solution was centrifuged at 300 RCF for 10 min at RT. In a washing step, the cell pellet was resuspended in Roswell Park Memorial Institute 1640 media (RPMI 1640, Fisher Scientific) and centrifuged (300 rcf, 10 min). The cell pellet was resuspended in BMDC complete media composed of RPMI 1640, 10% heat-inactivated FBS, 20 ng/mL granulocyte-macrophage colony-stimulating factor (GM-CSF, donated by the Cahalan Lab), 2 mM L-glutamine (Life Technologies), 10,000 U/mL penicillin, 10 mg/mL streptomycin, 25 μg/mL amphotericin B, and 50 μM beta-mercaptoethanol. Harvested cells were plated at $1x10^6$ cells/mL in 100 mm petri dishes (10 mL total media) and incubated at 37 °C in a CO_2 incubator (day 0 of cell culture). On day 3, 10 mL of fresh BMDC primary media was added to each petri dish. On day 5, BMDCs were released by repeated pipetting, centrifuged at 300 RCF for 10 min at RT, and plated in 24-well plates at $1.2x10^6$ cells/mL for cell surface marker activation, cytokine profile flow cytometry, and confocal microscopy experiments.

In vitro cell studies

RAW-Blue assays

RAW-Blue macrophages were plated at 50,000 cells/well in black-walled 96-well plates (Nunc) in complete test media. Stock solutions of agonists were prepared in complete test media

and sterile-filtered through a 0.2 μm filter immediately prior to addition to cell media. The agonists were added to the cell media at the final concentration indicated, with a total volume per well of 200 μL. For light-controlled experiments, cells were exposed to UV light immediately following addition of agonist. Optical sealing tape was affixed to the well plate and the light source was placed on top of the plate. Treated cells were incubated at 37 °C with 5% CO_2 for 18 h. After the incubation period, supernatant was analyzed for SEAP expression using QUANTI-Blue detection medium according to the manufacturer's protocol.

Fibroblast imaging

Fibroblasts were plated in coverslip-bottom 8-well plates (Thermo Sci.) at 5,000 cells/well in complete media and cultured for 48 h. One hour prior to imaging, media was exchanged for complete test media and the cells were equilibrated for 30 min at 37 °C with 5% CO_2 prior to adding agonist and imaging. Cells were treated with agonist at t=0 and imaged for 3 h at 37 °C with 5% CO_2. For light-controlled experiments, cells were exposed to UV light immediately following addition of agonist. The light source was placed underneath the coverslip wells. Following light exposure, cells were incubated at 37 °C with 5% CO_2 until imaging.

NF-kB activation of subpopulations of fibroblasts was performed similarly. Cells were plated and prepared as before. Light masks were made from black PEEK film (0.25 mm thick), with circular pinholes (area = 3.1 mm^2). The masks were aligned and affixed with tape to the bottom of the coverslip-bottom well plates. The plates were left undisturbed for 5 min following light exposure through the pinhole. Following light exposure, cells were incubated at 37 °C with 5% CO_2 until imaging.

The degree of NF-kB activation was determined by calculating the nuclear intensity of DsRed using ImageJ analysis of fluorescent images. The raw images were split into red and green

fluorescent channels. The fluorescence of the H2B-GFP (green channel) was used to set the limits of the nuclei. The green fluorescent channel was first processed by noise despeckling, median filter (2 px), and Gaussian blur (2 px). The threshold of the green fluorescent channel was set and watershed to create a binary image of individual particles (nuclei). Particles in this channel were measured, with the minimum particle size set equal to the minimum pixel area of a nuclei (varies between images sizes). To determine the amount of p65-DsRed in the nucleus, the measurement (mean intensity) was then redirected to the red fluorescent channel. The mean intensity of the entire red fluorescence image was also measured in order to normalize data and compare time points. The nuclei mean intensity was averaged and normalized to the mean image intensity.

Endocytosis assay

BMDCs were washed with RPMI. The cell pellet was resuspended at approximately $2x10^4$ cells/μL complete media supplemented with 10% heat-inactivated FBS. Agonist and protected agonist solutions were prepared in FITC-dextran-containing complete media supplemented with 10% heat-inactivated FBS. To visualize endocytosis following activation by an agonist, cells were imaged as time series (100 frames, 3.15 μs pixel dwell) on a Zeiss 780 confocal microscope using a 63x oil immersion. The BMDC suspension was combined with the agonist solution containing FITC-dextran 1:1 by volume, sandwiched between glass coverslips, and imaged without further incubation. For deprotection of **6**, the samples were exposed to UV light by opening the mercury lamp (120 W) shutter for 2 min.

Cell labelling protocol

Labelling of BMDCs and fibroblasts was accomplished by incubation of cells with caged TLR2/6 agonist **8.** A total of $1x10^7$ cells were added to a 15 mL centrifuge tube and diluted to a total volume of 10 mL in complete DMEM media. The caged agonist **8** was added at a final

concentration of 10 nM and the cells were allowed to incubate for 3 h with constant agitation. The cells were extensively washed with FACS buffer (PBS, 10% HI-FBS, 0.05% EDTA). In a typical wash step, the labelled cells were centrifuged (300 rcf, 10 min, 0°C), media or buffer removed, and suspended in 10 mL FACS. This process was repeated 5 additional times. Cells were suspended in 1 mL DMEM complete media and counted by flow cytometry. For BMDCs and fibroblasts, cells were seeded in a 24-well plate format at a total cell density of $2x10^5$ cells/well ($1x10^5$ cells/well of each cell type) according to the reported data. DMEM complete media (500 μL) was added to each well immediately followed by the light exposure steps outlined above.

APPENDIX B

TLR4 agonist **1**

^{1}H NMR (500 MHz, DMSO-d6) δ ppm 1.12-1.28 (m, 5 H), 1.53-1.75 (m, 5 H), 3.53 (broad s, 1 H), 3.91 (s, 2 H), 7.28 (t, J = 7.28 Hz, 1 H), 7.48-7.63 (m, 6 H), 8.09 (d, J = 8.09 Hz, 1 H), 8.20 (d, J = 8.19 Hz, 1 H), 12.13 (s, 1 H). ^{13}C NMR (500 MHz, DMSO-d6) δ ppm 24.93, 25.66, 32.85, 37.25, 48.44, 113.35, 119.75, 120.55, 120.84, 127.80, 130.04, 130.35, 136.56, 137.72, 139.41, 153.03, 155.44, 166.22. HRMS calc'd for $C_{24}H_{24}N_4O_2SNa$ $(M + Na)^+$, 455.1512; found, 455.1511.

Caged TLR4 agonist **2**

^{1}H NMR (500 MHz, DMSO-d6) δ ppm 1.11-1.15 (m, 3 H), 1.31-1.37 (m, 2 H), 1.58-1.66 (m, 3 H), 1.92-1.93 (m, 2 H), 3.68 (s, 3 H), 3.79-3.81 (m, 1 H), 3.88 (s, 2 H), 3.98 (s, 1 H), 5.95 (s, 2 H), 7.01 (d, J = 7.01 Hz, 1 H), 7.38-7.40 (m, 2 H), 7.54 (t, J = 7.54 Hz, 1 H), 7.63-7.64 (m, 3 H), 7.72-7.75 (m, 2 H), 7.80 (s, 1 H), 8.13 (d, J = 8.13 Hz, 1 H), 8.44 (d, J = 8.451 H). ^{13}C NMR (500 MHz, DMSO-d6) δ ppm 24.63, 25.43, 29.76, 32.92, 36.32, 48.57, 56.38, 56.84, 67.18, 107.78, 111.41, 116.25, 117.83, 120.58, 123.00, 124.47, 126.57, 129.05, 130.00, 130.54, 130.89, 135.62, 139.53, 140.34, 144.92, 148.11, 150.96, 153.91, 153.97, 159.70, 167.10. HRMS calc'd for $C_{34}H_{33}N_5O_8SNa$ $(M + Na)^+$, 694.1948; found, 694.1942.

TLR7 agonist **5**

^{1}H NMR ($CDCl_3$, 500MHz) δ 8.23 (d, *J* = 7.4 Hz, 1H), 8.05 (d, *J* = 8.7 Hz, 1H), 7.89 (s, 1H), 7.84 (d, *J* = 8.0 Hz, 1H), 7.68 (dd, *J* = 14.9, 7.7 Hz, 2H), 7.63 (t, *J* = 7.4 Hz, 1H), 7.57 (t, *J* =

7.5 Hz, 1H), 7.42 (t, *J* = 7.4 Hz, 1H), 4.52 (t, *J* = 7.2 Hz, 2H), 4.39 (d, *J* = 6.8 Hz, 2H), 3.87 (dd, *J* = 13.2, 6.8 Hz, 1H), 2.49 – 2.36 (m, 1H), 1.51 (d, *J* = 6.9 Hz, 3H), 1.10 (d, *J* = 6.4 Hz, 6H); ^{13}C (CDCl3, 500MHz) δ 150.44, 144.34, 142.92, 137.33, 136.95, 133.31, 132.76, 132.15, 128.33, 127.44, 126.89, 124.99, 124.27, 123.54, 120.09, 119.82, 69.15, 55.23, 33.34, 28.88, 19.86, 17.94; MS m/z calc'd for $C_{24}H_{25}N_5O_4$ [M+Na] 470.18; Observed [M+Na] 470.1.

TLR7 and 8 agonist **6**

^{1}H NMR ($CDCl_3$, 500MHz) δ 8.31 (s, 1H), 8.22 (d, *J* = 8.4 Hz, 1H), 8.18 (d, *J* = 8.1 Hz, 1H), 7.84 (d, *J* = 8.0 Hz, 1H), 7.71 – 7.61 (m, 4H), 7.53 (t, *J* = 5 Hz, 1H), 7.42 (t, *J*= 5 Hz, 1H), 4.96 (s, 3H), 4.84 (s, 2H), 4.52 (d, *J* = 6.5 Hz, 2H), 3.85 (dd, *J* = 13.3, 6.7 Hz, 1H), 3.72 (d, *J* = 7.1 Hz, 2H), 1.50 (d, *J* = 6.9 Hz, 3H), 1.38 (s, 6H), 1.32 (d, *J* = 6.8 Hz, 3H). ^{13}C (CDCl3, 500MHz) δ 174.49, 151.45, 150.59, 150.38, 144.53, 143.93, 137.41, 135.44, 132.84, 130.47, 128.39, 128.49, 124.59, 124.33, 119.82, 116.82, 110.00, 71.50, 69.07, 66.76, 64.96, 56.47, 33.43, 29.76, 27.97, 18.15; MS m/z calc'd for $C_{27}H_{31}N_5O_6$ [M+Na] 544.21; Observed [M+Na] 544.21.

In vitro cell studies

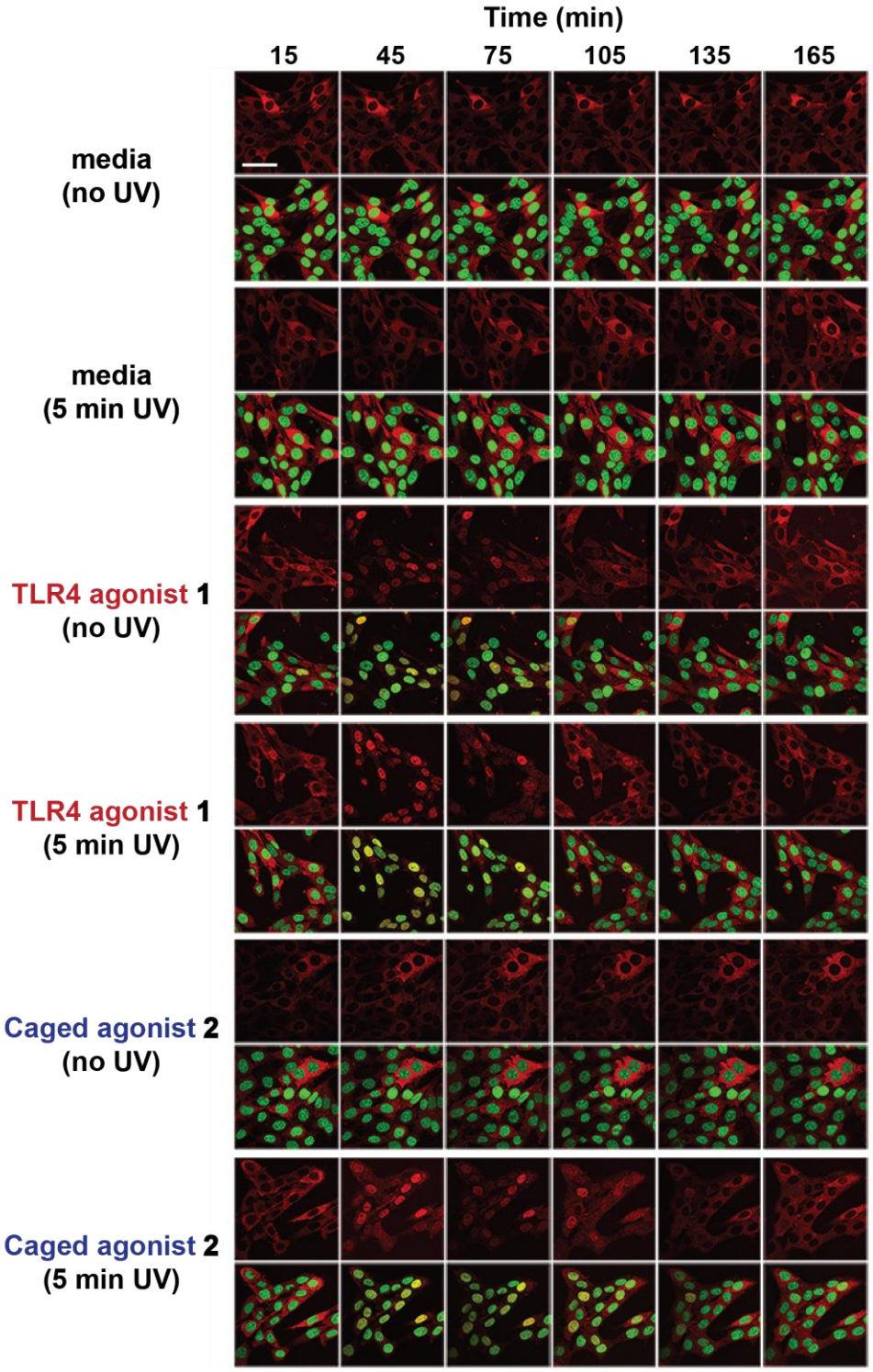

Figure 7.1. Time course of NF-κB activation in fluorescent reporter cells. Fibroblasts expressing p65-DsRed (NF-κB) and H2B-GFP (nuclei) were treated at t=0 with media, **1** or **2**, with and without 5 min light exposure (15 W, 365 nm), and images by fluorescence microscopy for up to 3 h. Scale bar is equal to 50 μm.

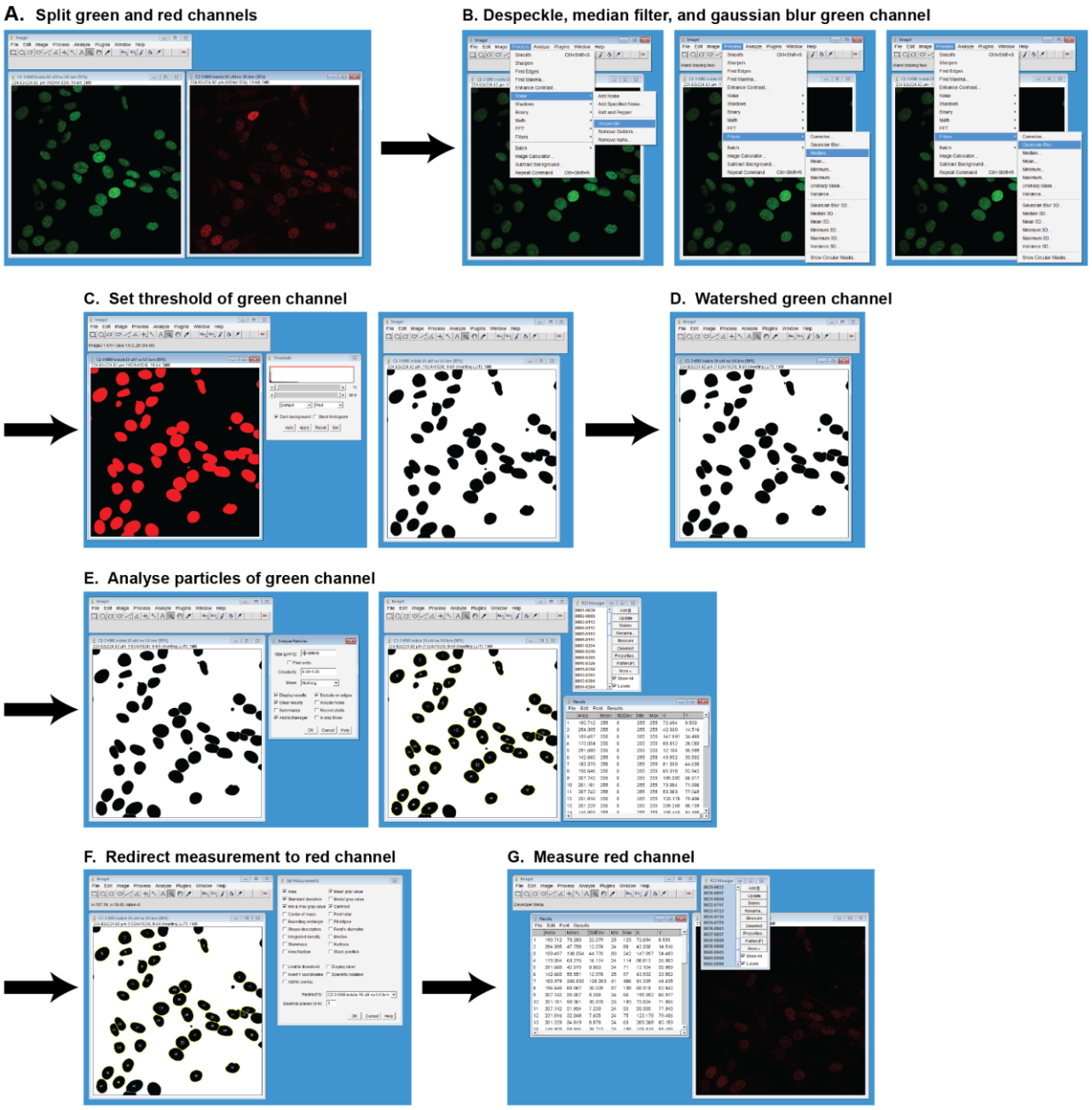

Figure 7.2. Flow diagram of ImageJ analysis for quantifying NF-κB activation in fluorescent reporter cells. The fluorescence of the H2B-GFP (green fluorescent channel) was used to set the limits of the nuclei (**B-E**). The amount of p65-DsRed in the nucleus is determined by redirecting the measurements to the red fluorescent channel (**F-G**).